Addis Ababa University

Addis Ababa Institute of Technology

School of Multidisciplinary Engineering

Center for Materials Engineering

Selective Electrochemical Reduction of Carbon dioxide on CuS (001) Surface using Density Functional Theory

Thesis Submitted to Center for Materials Engineering in Partial Fulfillment of the Requirements for the Degree of Master of Science in Materials Engineering

By

Nigussie Birhanu Beyene (M.Sc.)

October, 2020

Addis Ababa, Ethiopia

Addis Ababa University

School of Graduate Studies

Addis Ababa Institute of Technology

Selective Electrochemical Reduction of Carbon dioxide on CuS (001) Surface using Density Functional Theory

By

Nigussie Birhanu Beyene (M.Sc.)

A Thesis Submitted to Center of Materials Engineering in Partial Fulfillment of the Requirements for the Degree of Master of Science in Materials Engineering

Approved by Board of Examiners

Georgies Alene (Ph.D.)	_____	
Advisor	Signature	Date
Tekalign Debela (Ph.D.)	_____	
Co. Advisor	Signature	Date
Yedilfana Setarge (Ph.D.)	_____	
External Examiner	Signature	Date
Sintayehu Nibret (Ph.D.)	_____	
Internal Examiner	Signature	Date

DECLARATION

I, the undersigned, hereby declare that this thesis is my original work, has not been submitted in any previous application for a degree and that all sources of materials used for this thesis have been duly acknowledged.

Name: Nigussie Birhanu Beyene

Signature: _____

Date of submission: October, 2020

Abstract

Electrochemical carbon dioxide reduction reaction (ECR) on surface CuS (001) is one of the most capable approaches to convert CO_2 gases to formic acid and carbon monoxide products. Geometry optimization and Gibbs free energy calculation were carried out using density functional theory with general gradient approximation of Perdew–Burke–Ernzerhof (PBE) as implemented in quantum ESPRESSO and VASP software package with computational hydrogen electrode (CHE) approaches. In this work the bulk CuS, CuS (001) surface and adsorbate configuration structures of intermediate species (*H, *OCHO, *COOH, and *CO) and reduction mechanisms were optimized geometry structure and calculated Gibbs free energy. Herein, the two elementary reaction paths are proposed * + CO_2 $\rightarrow$ *OCHO $\rightarrow$ HCOOH, and * + CO_2 $\rightarrow$ *COOH $\rightarrow$ *CO + H_2O $\rightarrow$CO for the formation of formic acid and carbon monoxide and their activation barrier energy for intermediate *OCHO, *COOH_Cu, *COOH_S, *CO_Cu, and *CO_S are -0.03eV, +0.74 eV, +1.47 eV, -0.32 eV, and -1.05 eV respectively at 0V vs RHE. Intermediate *OCHO and *COOH_Cu have smallest activation barrier energy than the others. This study revealed that easier reaction would be occurred on *OCHO and *COOH_Cu intermediate. So that CuS (001) surface has highly selective catalyst and favourable to the formation of formic acid and good selective to carbon monoxide through *OCHO and *COOH-Cu intermediate, respectively.

Keywords: Density functional theory, Electrocatalysts, Electrochemical reduction of CO_2 reaction, selectivity

Acknowledgment

First of all, I would like to express my deep gratitude and thanks to the Sovereign Lord for His Grace, Mercies, Goodness, Compassion, Guidance, Protection and Strength He has shown me through this thesis work.

Firstly, I would like to express my sincere gratitude to my advisor Dr. Georgies Alene for his continuous support, patience, motivation, and immense knowledge. His guidance and valuable feedback helped me in all the time of research and writing of this thesis.

Equivalently, I am very thankful to Dr. Tekalign Debela (co-advisor) for his essential help. He is research professor at department of Nano and advanced materials, College of engineering, Jeonju University, republic of Korea .He taught me a lot and corrected my mistakes with much patience and who motivated me and shared research technique with me. I am also thankful to Tadesse Shewaye computer expert at NIB international bank for providing me a connection to the UNIX system to use Quantum Espresso. This accomplishment would not have been possible without them. Thank you.

Table of Contents

List of Tables

List of Figures

Abbreviation

BO	Born-Oppenheimer
CH_4	Methane
CHE	Computational hydrogen electrode
CO	Carbon monoxide
CO_2	Carbon dioxide
CRGE	Climate Resilient Green Economy
Cu	Copper
CuS	Covellite (Copper Sulfide)
DFT	Density functional theory
ERC	Electrochemical reduction of carbon dioxide
ESPRESSO	opEn-Source Package for Research in Electronic Structure, Simulation, and Optimization
eV	electron volt
GDP	Gross Domestic product
GGA	General Gradient Approximation
H_2	Hydrogen gas molecule
HCOOH	Formic acid
HER	Hydrogen evolution reaction
IMF	International Monetary Fund
LDA	Local density Approximation
MS	Materials Studio

NC-PP	conserving pseudopotentials
PAW	Projected Augmented wave
PBE	Perdew-Burke-Ernzerch
PPM	part per million
PWscf	Pane-wave self consistent field
QE	Quantum-ESPRESSO
RHE	Reverse hydrogen electrode
R_y	Rydberg
S	Sulfur
US-PP	Ultrasoft pseudopotentials
VASP	Vienna Ab-initio Simulation Package
VESTA	visualization for electronic and structural analysis
ZPVE	Zero-point vibrational energy

Chapter One

1. Introduction

1.1.Background of the study

Human activity, especially consumption of fossil fuels, is altering the planet. The amount of carbon dioxide (CO_2) in the air has been increasing which may adversely affect the environment and global challenges facing the human. CO_2 is largest contributor amongst the greenhouse gases that associated with a rise in the global average temperature, break the balance of the carbon cycle in nature and cause to the warming of Earth's atmosphere, and is considered main contributor of global climate change [1] [2][3]. In July 2019,the concentration of CO_2 in the atmosphere is getting very high values >408 ppm, showing an increasing trend at a current annual rate of 2.56 ppm per year [4].The following figure 1 shows annual means global growth rate of CO_2 between 1960 and 2020 year of the planet.

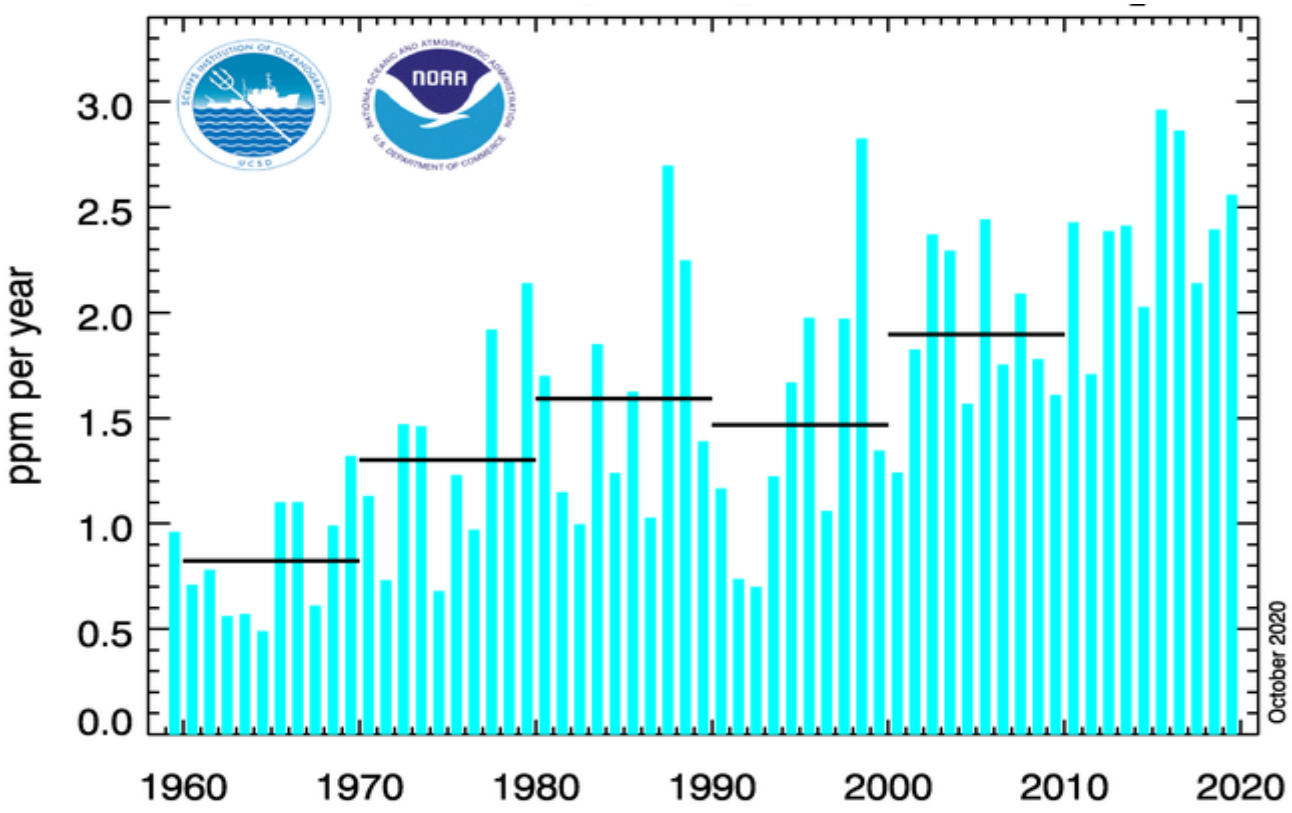

Figure 1 Annual Mean global growth rate of CO_2 [5]

Burning of fossil fuel such as natural gas, oil, coal for production of energy has claimed to be the major source to drastically increase CO_2 emission into the atmosphere which leads to future global

warming and ecological crisis, but human society will still depend heavily on fossil fuel. Development of industries, population growth, human activity, longer life expectancy increase use of fossil fuels for energy and feedstock supplements is severe for resource, environment and climate of the world [6][7]. The reduction of CO_2 concentration in the atmosphere represents one of the worldwide problems for the last and next decades because of numerous negative effects related to global warming. Large struggle have been dedicated to reducing the concentration of atmospheric CO_2.The development of systems capable of reducing CO_2 can help establish a carbon-neutral economy. Finding ways to reduce CO_2 amount from the atmosphere is of great significance [8] [9].

Therefore, it is necessary to develop new energy utilization technologies and improve the efficiency of conversion and utilization of fossil energy to alleviate severe energy shortages and environmental problems. Converting CO_2 into industrial chemicals and fuels by thermochemical, photochemical, and electrochemical, etc., are attractive methods. Among these ways, electrochemical reduction of CO_2 (ERC) reaction is a promising technology for converting waste CO_2 into fuels and feedstock is regarded as an attractive strategy that is safe and economical as it is a process that can contribute to mitigate climate change. Electrochemical reduction is a promising approach for converting CO_2 into formic acid (HCOOH), carbon monoxide (CO), methan (CH_4) and other hydrocarbons and also simultaneously improve energy crisis and reduce the global carbon emission [10][11].

Copper, Indium-Zinc, Molybdenum sulfides and Selenides have shown excellent electrocatalytic activity for CO_2 reduction reaction into HCOOH and CO. Formic acid finds its applications in textiles, pharmaceuticals and food chemicals, due to its strong acidic nature and reducing properties. Formic acid is a very useful liquid fuel that can be converted to longer chain alcohols. Copper sulfide as a low-toxicity and emerging material has wide prospects in the area of CO_2 reduction due to its distinctive structural and electrochemical properties. It is a well-known chemical that has potential as hydrogen carrier and as fuel for fuel cells [12] [13][14].However, there are still many challenges to develop high performance catalyst to carbon dioxide reduction such as higher activity, stability, overpotential required for this reaction due to the formation of high energy barrier reaction intermediates and inability to control the product selectivity. The solution to solving these problems is to develop high performance electrocatalysts with good activity, selectivity and stability. Copper sulfides have promising prospects for improving catalytic activity and product selectivity in CO_2 reduction. Therefore CuS material has showed good selectivity, high activity and received attention in electrochemical reduction of CO_2 into hydrocarbon with high Faraday efficiency [15][16][17].

In this study, the electrochemical reactions on CuS (001) surface are modeled using theoretical methods which employ the use of a computational hydrogen electrode (CHE) model with DFT calculations [18][19]. In this work, we performed structures of bulk and surface of copper sulfide, calculated activation energy, predicted reaction path and mechanism of reduction CO_2 to various intermediates such as H, CO, OCHO and COOH and comparisons can be drawn between various catalytic changes in Gibbs free energy/activation energy of intermediates species to the formation of HCOOH and CO.

1.2. Statement of the problem and limitation

The use of fossil fuels for energy production emits a large amount of CO_2 into the atmosphere, causing global environmental problems, such as global warming, sea level rise, land desertification, etc. Compared to the preceding five-year assessment period 2011–2015, the current five-year period 2015–2019 has seen a continued increase in CO_2 emissions and an accelerated increase in the atmospheric concentration of major greenhouse gases, with growth rates nearly 20% higher. The increase in the oceanic CO_2 concentration has increased the ocean's acidity. The global budget of anthropogenic carbon has continued to grow since 2019 annual rate of 2.87 ppm per year due to the increase in CO_2 emissions from the combustion of fossil fuels (coal, oil and gas) and industry products [20][21].

The burden of climate change is real for poor countries that decline in crop yields due to climate change in agriculture-based economies. This implies devastating effects on developing economies that depend heavily on agriculture. In Ethiopia, agriculture supports the livelihoods of the majority of people and provides 80% of employment International Monetary Fund (IMF) report. It generates about 90% of export revenues, supplies 70% of raw materials for domestic agro-industries and contributes 43% of the gross domestic product (GDP)[22] .Consequently, any negative environmental shock to the agricultural sector can cause devastating impacts on the whole economy. CO_2 emissions have a negative impact on the production of major agricultural export commodities. The main agricultural export commodities are included coffee, oilseeds, pulses and khat. With Climate Resilient Green Economy (CRGE), production of primary export commodities declines from baseline 22.78 billion Birr by 8.3% to 20.88 billion Birr by 2030 [23].

This thesis work focus to investigate CO_2 emissions reduction strategy due to its great impact in climate change. Great efforts have been devoted to reducing the concentration of atmospheric CO_2.Different studies show that high overpotential, low activity for the formation of the desired products, instability at reducing conditions and low selectivity towards the desired products are main

problems in electrochemical CO_2 reduction mechanism[24]. There is no DFT computational research study has been carried out using CuS reduction of CO_2.For most electrocatalysts, however, the inertness of CO_2 molecules and complex multi- electron transfer steps involved in CO_2 reduction reaction result in large thermodynamic barriers, low selectivity toward specific products[25][26]. In this regard, it is needed to develop highly selective and low activation energy electrocatalysts for CO_2 reduction reaction. The scope of this study is only on theoretical properties based on DFT without any experimental work.

1.3. Objectives

1.3.1. General objective

The main aim of this work is to study electrochemical reduction of carbon dioxide using copper sulfide catalyst to formic acid and carbon monoxide by means of density functional theory calculation with computational hydrogen electrode model.

1.3.2. Specific objectives

- To investigate optimized geometry electronic structure of bulk CuS and pristine slab CuS (001) structures which is suitable functional materials for carbon dioxide reduction
- To determine key elementary steps and mechanism of CO_2 reduction
- To calculate intermediate activation energy and adsorption energy of H, OCHO, COOH, CO using Gibbs free energy equation

Chapter Two

2. Literature Review

Density functional theory calculations in combination with the computational hydrogen electrode model have been used to explain reaction mechanism and described activation energy of intermediate that are involved in the reduction of CO_2 materials. Theoretical models have been used to search for catalysts with improved electrocatalytic activity and selectivity. ERC is of importance as a prospective component of a carbon energy cycle. ERC converted into different chemicals and fuels provides good pathway for environmental and energy sustainability [13] [27].

2.1.Electrochemical Reactions

Electrochemical reactions entail the transfer of electrons to or from a molecule, atom, or ion at an interface between an electronic conductor, the electrode (through which the electrons reach or leave the interface), and an ionic conductor (through which the ions travel). There are two fundamental types of half cell reactions such as oxidation reactions and reduction reactions. Reduction is involves the transfer of electrons from the electrode to the species. A cathodic side reaction is hydrogen generation by

$$\text{Reduction: } H^{+2} + 2e^- \rightarrow H_2 \quad \text{.....2.1}$$

Addition of electrons to a species is reduction in the chemist's terminology and reaction [2.1] is termed a cathodic one; while this reduction is occurring at an electrode we term it a cathode [28].

2.2.Fundamentals of Electrochemical CO_2 Reduction

Reduction of CO_2 to important fuels and chemicals is an attractive method that is safe and economical. There are different conversion method of CO_2 to fuels such as electrochemical, thermochemical and photochemical. Among these methods to reduce CO_2 emissions from the use of fossil fuels, the electrochemical conversion of CO_2 into fuel products is being considered an attractive technique to reduce the reliance on fossil fuels [1][8][13].

ERC is an attractive way to convert CO_2 because of the following advantages (1) water is the proton source; (2) high equilibrium conversion at ambient temperature and pressure; and (3) relatively simple and green .These advantages are increasing attention and go through rapid development in using electrocatalyst for CO_2 reduction to different carbon products. Achievement of growth of high capability product CO_2 reduction strongly relies on electrocatalyst and other methods [29][30].

Copper, both metallic and in oxides form, is considered a promising electrode material as it offers intermediate hydrogen overvoltage and produces more reduced form of carbon dioxide, such as

methanol, ethane, methane, and ethylene. As the potential becomes more negative, the generated carbon monoxide/formate suppresses hydrogen evolution. ERC on Cu-based materials has received growing interest in recent years. Early electrokinetic experiments by Hori and co-workers using both single-crystal Cu electrode surfaces and polycrystalline Cu foils found that methane and ethylene are the major CO_2 reduction products at higher overpotentials, while CO and formic acid (HCOOH) along with a large amount of hydrogen are the major products at lower overpotentials [12] [13].

Metal nanocatalysts have the potentials to selectively reduce CO_2 to one carbon product such as CO, formic acid, or a hydrocarbon[31]. Metals that bind CO and hydrogen strongly, such as Pt and Ni, are selective for evolution of hydrogen. Copper is the only metal with moderate CO and hydrogen binding energies, and is the only transition metal that selectively catalyzes the reduction of CO_2 to hydrocarbon.

Metal and metal-based catalysts have been used for electroreduction of CO_2 to CO, hydrocarbons and alcohols. Some electrocatalysts, such as precious metal and copper-based catalysts, have shown to be promising for electroreduction of CO_2 to methanol. Among these materials, Cu has been reported as the promising electrocatalyst that is active and selective for CO_2 reduction to hydrocarbons and alcohols. Many alloy/nonmetal catalysts have also been developed, with promising results for CO and HCOOH production, and formate is reported as a potential first commercial product [32] [33].

Table 1 The electrochemical reduction products of CO_2 over various catalysts.

Catalysts	products
Solid oxide fuel cells	
Platinum	CO
Nickel	CO, methane CO
Palladium	CO
Copper	CO
Metallic electrodes in aqueous solution	
Copper	Hydrocarbons, CO, formate, alcohols,
Platinum	CO, methanol
Others (Pb, Oxide-derived Au)	CO, formate
Molecular electrocatalysts	
Copper complexes	oxalate
Palladium complexes	CO, formic acid
Nickel complexes	CO, oxalate, formic acid, formaldehyde
Cobalt complexes	CO, formic acid, alcohols

HCOOH is a very useful liquid fuel that can be converted to longer chain alcohols. Hence, much effort has been devoted to ERC to HCOOH ($CO_2 + 2H^+ + 2e^- \rightarrow$ HCOOH; E = -0.608 V vs. NHE at pH 7) using several transition and post-transition metals including Pb, Hg, In, Sn, Cd, Bi, and Ti as selective catalysts. The hydrogen evolution reaction (HER, $2H^+ + 2e^- \rightarrow H_2$) also occurs as a competitive reaction, and its inhibition is essential for obtaining high efficiency for the CO_2-to-HCOOH pathway. Pure metals such as Cd and Hg are using in electrocatalyst in ERC of selective formic acid product. The Formic acid is a dominant product of on the Pb based electrode. [34][29]

2.3.Mechanism of electrochemical reduction of CO_2

CO_2 is a thermodynamically most stable molecule due to the strong C = O double bond with bonding energy of 750 kJ mol^{-1}. Considerably larger than that of C – C= 336 kJ mol^{-1}, C -O =327 kJ mol^{-1}, or C- H bond 411 kJ mol^{-1}. CO_2 reduction through the electrocatalytic method is a thermodynamically uphill reaction and demands significant energy input to break the C=O bond. To make it even more complicated, CO_2 reduction may proceed via several different reaction pathways with the transfer of 2, 4, 6, 8, 12 or even more electrons and yielding different products including Carbon monoxide (CO), formic acid (HCOOH), methane (CH_4), ethylene (C_2H_4) etc. Its multi step reduction through the electrochemical method is extensively more difficult than the splitting of water. It has an important input of energy, optimized reaction conditions and active catalysts are necessary for any chemical conversion of CO_2 to a fuel. However, the conversions of chemical reaction are driven by differences in the Gibbs free energy between the reactants and products of a chemical reaction under certain conditions. Prominently, one can then take the enthalpy term as a good initial guide for assessing thermodynamic stability and feasibility of any CO_2 conversions. [3][30][35]

The detailed mechanistic pathways for each product are not clear at present, and in many cases several different schemes have been proposed. Figure 2 shows the most commonly proposed pathways for ERC to carbon monoxide, formic acid, formaldehyde and methanol.

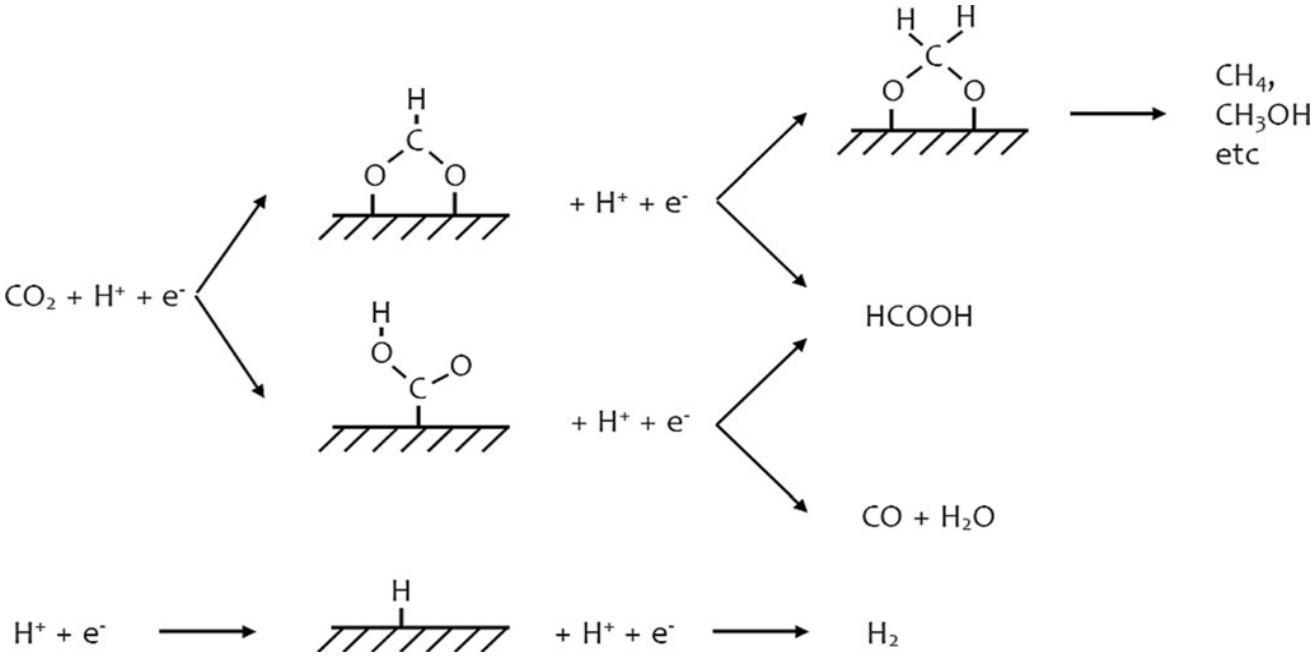

Figure 2 Reaction pathways for the electroreduction of CO2 to different products (top), and the competing hydrogen evolution reaction (bottom)[36].

As shown in Figure 2 the reaction start by identifying relevant reaction pathways for the electroreduction of CO_2 and the HER, the transfer of a first proton/electron pair to CO_2 leads to a formation of either the formate (*OCHO) or carboxyl (*COOH) species. Both *OCHO and *COOH can be reduced to HCOOH and CO upon the transfer of a second proton/electron pair [36].

Mechanism of ERC to hydrocarbons on Cu (111) the first elementary step of CO_2 reduction reaction is the addition of a proton to CO_2 and extraction of an electron from the electrode to form ∗COOH (an asterisk, *, indicates adsorption to the surface). Since full electrochemical simulations as the ones described above where the solid/liquid interface is modeled and activation energy evaluated as a function of applied voltage are computationally demanding it is important to develop a simple descriptor that can help identify the more promising catalyst materials. However, in order to predict the selectivity towards a given product, calculations of the activation energy in the various elementary steps needs to be carried out to evaluate the reaction rates as a function of applied potential. The activation energy of proton-electron transfer reaction steps is strongly dependent on the strength of the applied potential.[9]

In the presence of CO_2, intermediates formed from the reduction of CO_2 may be adsorbed on the surface. Initially, we focus on intermediates formed by 1 or 2-electron reduction of CO_2. Protonation of CO_2 may happen at an O atom leading to carboxyl: $* + CO_2 + (H^+ + e^-) \rightarrow COOH*$, which may be further reduced to CO: $COOH* + (H^+ + e^-) \rightarrow CO* + H_2O$. Alternatively, CO_2 may be protonated at the C atom to produce formate: $* + CO_2 + (H^+ + e^-) \rightarrow OCHO*$, this may be further protonated to formic acid: $OCHO* + (H+ + e-) \rightarrow HCOOH$ [25]

2.4.Structural Properties of Crystal Covellite (CuS)

Covellite (CuS) bulk structure belongs to family of layered chalcogenide materials and crystallizes with P63/mmc (NO.194) space group, showing hexagonal unit cell at room temperature, with 12 atoms in the unit cell, its lattice parameters are: a=3.796 and c=16.382, giving a calculated density of $4.66 g.cm^{-3}$ [37]. It has two alternating layer: CuS_3 units (triangular planes) and CuS_4 units (tetrahedron) and link of S-S bond the structure is important in chemistry of sulfide. Covellite (CuS) is a green-black binary copper sulfide mineral which mainly occurs after supergene enrichment processes in copper ore deposits It is besides its natural occurrence, covellite can also be grown by artificial routes, e.g., in solution or using solid vapor reactions[38][39][40].

Covellite is a metallic layered mineral with rather strong interlayer interaction. The unit cell can be seen as slabs connected by S−S bonds. It is unstable but can be stable using supports and have graphene-like structure. CuS received much attention because of their opto-electronic properties and due to this property applied to catalyst application [41][42][43].

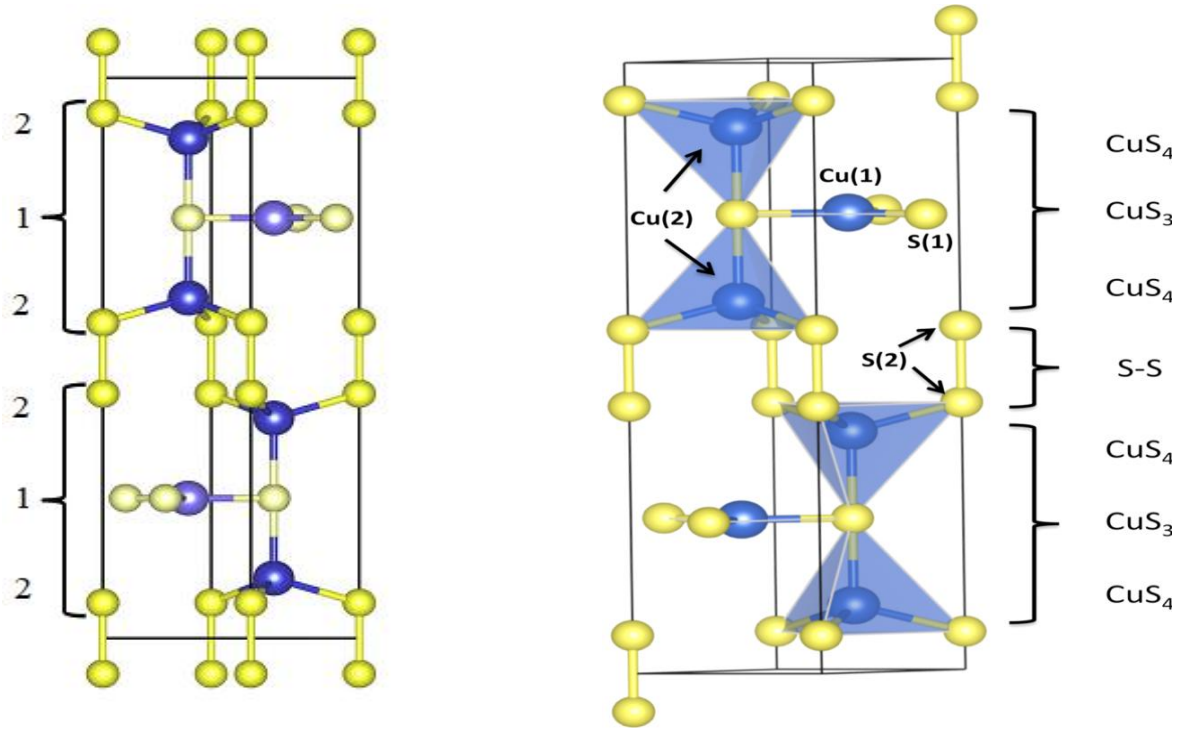

a **b**

Figure 3 Structural aspects of covellite hexagonal unit cell (CuS) showing links of the Cu - S and S-S bonds. Number 2 and 1 denotes copper in tetrahedral and trigonal planar configuration in geometry. Style a) ball and stick, b) polyhedral. Blue and yellow spheres are copper and sulfur atoms, respectively[42][43]

In above figure 4 arrangement of sulfur atoms around Cu (1) is trigonal and that around Cu(2) is tetrahedral. These two coordination types are most common in sulfides. Trigonal planar and tetrahedral arrangements of copper atoms coupled to two different binding sites of the sulfur atoms of covellite have been widely investigated due to their electronic, structural, and bonding properties. The copper atom in CuS is less toxic than other atoms (e.g., Pb, Cd, As) into other semiconductors.

Table 2 Calculated and experimental lattice parameter, interatomic bond length, bond angle and cell volume for CuS [44] [45].

lattice parameter, bond angle	**Exp.**	**GGA**
a=b (Å)	3.7938,3.76	3.826
C (Å)	16.341	16.596
Cu(1)-S(1) (Å) x3	2.190s	2.208
Cu(2)-S(1) (Å)	2.331	2.374
Cu(2)-S(2) (Å) x3	2.305	2.322
S(2)-S(2) (Å)	2.071	2.113
S(1)-Cu(2) -S(2)	108.16	
V_0 (Å^3)	202.5,199.9	208.13

Analysis of chemical bonding and calculated structural properties are compared with the available experimental data in Table 2. The Cu (2)−S(1) and S(2)−S(2) bonds are overestimated by less than 0.043 and 0.042 Å, respectively, for the GGA level of theory compared with the experimental values.

2.5. Copper sulfide used to electrochemical carbon dioxide reduction

Copper sulfide compound has been continuously selected as a catalyst for electrochemical reduction, especially for CO_2 reduction. The obtained CuS/Cu electrode was very efficient in reducing CO_2 to HCOOH. Sulfur- modified copper catalysts have a strong selective to formate formation in CuS ECR with more recent work finding CuS as an active, selective, cheap catalyst for formic acid. The presence of sulfur weakens the *COOH and HCOO* adsorption energies, which suppress the formation of *COOH toward CO and reduce the energy of the potential-limiting step for formate production. It enhances the formation of formate. For the copper sulfide catalyst, S is the main promoter of the catalytic performance. The doping of the S atom offers different electrochemical properties, increases the electro active surface area of the material and improves the ion and electron transport rate. The S atom has the ability to combine the hydride with the physical CO_2 adsorption

capability to form formate, and change the adsorption strength of the CO_2 reduction reaction intermediate to reduce the energy barrier. CuS/Cu electrode was very efficient in reducing CO_2 to HCOOH. Experimental result show that faradaic efficiency (FE) of formic acid production and the reduction current density could reach 85% and 5.3 mA/cm^2, respectively, at the potential of -2.0 V vs. Ag/AgCl. CuS as active, selective, cheap catalyst to formate [15] [46]

By combining DFT calculations and isotopic labeling operando Raman spectroscopy, indicate the presence of sulfur weakens the *COOH and HCOO* adsorption energies, which suppress the formation of *COOH toward *CO and reduce the energy of the potential-limiting step for formate production. [15]

Chapter Three

3. Computational Methodology

The main aspects of Density Functional Theory are the different approximation which makes DFT a feasible practice. We would discuss how we can translate and relate the DFT calculations, into some understandable form by using theoretical models, such as standard hydrogen electrode.

3.1. Density Functional Theory (DFT)

DFT is one of the standard computational tools in condensed matter physics, chemistry, and biochemistry to study the electronic structure of many-electron systems through electron density. It is called density functional theory because functional of electron density is used instead of the wave function to study properties of the many-body system. As electron density is used instead of the wave function, the multi-dimensional many-electron systems reduced to three dimensions; making the problem much easier.

The quantum mechanical behaviour of a system is explained by the Schrödinger equation [47]. The core of quantum mechanics is the Schrödinger equation H Ψ = E Ψ, where Ψ is the wavefunction. Once the wavefunction is known for a particular system, then any physical property may in principle be determined for that system. The Schrödinger wave equation is the partial differential equation for the electron‘s wave function Ψ. It is used to find properties of a bound electron with the help of conservation of energy principle. A solution of this equation gives a quantum number, size, and orientation of electronic orbitals. The time-independent Schrödinger equation for a single non-relativistic particle is given by

$$\left[-\frac{\hbar^2}{2m}\nabla^2 + V(r)\right]\psi = E\psi \quad \text{.....1}$$

$Where, \hbar = \frac{h}{2\Pi} = 1.054x10^{-34}\,Js$, is the reduced plank Constant

m=9.109x10^{-34} Kg is the mass of the electron

∂^2 is the Laplacian (differential Operator)

V(r) =is the potential energy

Only upon like atom like H, He^+, etc., we can solve the Schrödinger wave equation to calculate the wave function and hence the allowed energy states of the system. The multi-dimensional nature of the partial differential equation makes it increasingly complex and difficult to solve Schrödinger equation

theoretically for systems greater than one or two electrons. In order to solve this problem, we must apply some approximation to reduce the number of degree of freedom of the system. DFT is a method that offers a computationally-derived solution for the non-relativistic time-independent Schrödinger equation based on the Hohenberg- Kohn theorems.

3.1.1. Born-Oppenheimer approximation

One of the most basic approximations is a Born-Oppenheimer approximation. This approximation helps to separate the motion of the nuclei and the motion of the electrons in the molecule. As a result, this approximation breaks the molecular wave function into the electronic and nuclear component. The time-independent, non-relativistic Schrödinger equation 3.1for multiple electrons interacting with multiple nuclei is:

$$[-\frac{\hbar^2}{2m}\sum_{i=1}^{N}\nabla_i^2+\sum_{i}^{N}V(r_i)+\sum_{i=1}^{N}\sum_{j\langle i}U(r_i,r_j]\psi=E\psi \quad \text{.....2}$$

Here, U (r_i , r_j) the potential due to the interaction between an electron at position r_i and another at position r_j, $\Psi = \Psi$ ($r_i \ldots r_N$) is the electronic wave function for all N electron and E is the ground state energy of the electrons.

The first term in this bracket in this equation define the kinetic energy of each electron, the second term defines the interaction energy between each electron and the third term defines the collection of atomic nuclei and the interaction energy between different electrons.

3.1.2. The Hartree-Fock Approximation

While the BO approximation separates the nuclear from the electronic contributions of the wavefunction, the electronic component itself remains too complex to solve, as it is a function of all the electron coordinates of the system. The Hartree product allows expressing this wavefunction as a product of wavefunctions for N individual electrons

$$\psi=\psi_1(r_1)\psi_2(r_2),\ldots,\psi_N(r_N) \quad \text{.....3}$$

An additional step to satisfy the anti-symmetry requirements that arise from the Pauli Exclusion Principle by expressing the product in the form of a Slater determinant. This guarantees an anti-symmetric product of non-interacting wavefunctions to describe the electronic wavefunction.

3.1.3. The Hohenberg-Kohn Theorems and the Kohn-Sham Equations.

Despite the reduction in complexity offered by the BO approximation and the Hartree-Fock approximation, the individual electron wavefunctions remain a computationally challenging problem. Hohenberg and Kohn provided two important theorems proving that the many-body problem may be reduced to a simpler problem of only three spatial coordinates by solving for the electron density in lieu of the electron wavefunctions (where 3N dimensions are needed for N electrons). The electron density, ρ(r), is a spatial quantity that is defined as a function of the individual wavefunctions:

$$\rho(r) = 2\sum_i \psi^*(r)\psi(r) \quad \text{.....4}$$

Hohenberg and Kohn's first theorem states that the ground state energy of a system, as determined by the Schrödinger equation, is a unique functional of the electron density**.** The second theorem states that the exact ground state density gives the lowest total energy. The electron density that can obtain the lowest energy is the electron density of the ground state [48][49]. Finding the energy functional minimum therefore guarantees the solution for the exact electron density of the system.

The Kohn–Sham equations have the form

$$\left[\frac{h^2}{2m}\nabla^2 + V(r) + V_H(r) + V_{XC}(r)\right]\psi_i(r) = \varepsilon_i\psi_i(r) \quad \text{.....5}$$

The exact form of the energy functional is unknown and remains a current challenge of DFT methods today. The energy functional, in terms of the electron density ρ(r), can be written as:

$$E(\rho) = T_e(\rho) + V_{ext}(\rho) + V_H(\rho) + E_{XC}(\rho) \quad \text{.....6}$$

Where $T_e(\rho)$ is the Kohn-Sham kinetic energy, $V_{ext}(\rho)$ is the external potential acting on the interacting system, and $V_H(\rho)$ is the Hartree Energy. The term $E_{xc}(\rho)$ is known as the exchange-correlation functional and includes the effects of exchange and correlation interactions between electrons as well any other effects, such as self-interaction corrections, which are not included in other known terms. Other than for free electron gas systems, the exact form of the exchange-correlation functional is not known. Several approximate forms are used for this term instead, such as the Local Density Approximation (LDA) and the Generalized Gradient Approximation (GGA) [47] [50].

3.2. Approximations to the exchange-correlation energy functional

3.2.1. Local Density Approximation

One of the problems in DFT is the exact exchange functional and correlations functional are unknown. Only for the free electron gases they are known. The local density approximation (LDA) is the first and most widely used approximation to the exchange-correlation energy. This approximation is based on the assumption that the exchange correlation energy of a real system behaves locally as in a uniform electron-gas having the same density. The functional is evaluated according to the formula below

$$E_{xc}^{LDA}[\rho] = \int \rho(\vec{r})\varepsilon_{xc}(\rho(\overrightarrow{r}))d\vec{r} \quad \text{.....7}$$

3.2.2. Generalized gradient approximation

According to LDA, density is same at every place. Due to this, exchange energy can be underestimated and correlation energy can be overestimated. To correct this error, commonly electron density is expanded in terms of density gradient. This correction is called generalized gradient approximations (GGA) it has the following form

$$E_{xc}^{GGA}[\rho] = \int \rho(\vec{r})\varepsilon_{xc}(\rho(\overrightarrow{r}),\nabla(\rho))d\bar{r} \quad \text{..... 8}$$

Impressively, this new formulation of the time-independent Schrödinger equation is a function of only three spatial variables, whereas Equation 3.1 is a function of 3N variables. The exchange-correlation energy functional is related to the term $V_{XC}(r)$ by

$$V_{XC} = \frac{\delta E_{XC}(r)}{\delta \rho(r)} \quad \text{.....9}$$

Iteratively solving for the electron density using the Kohn-Sham equations allows obtaining a self-consistent solution for the ground state energy.

3.3. Plane-wave periodic systems

Continuous periodic systems, such as solid crystalline structures, can be modeled by periodically repeating an irreducible unit, known as a supercell. For such periodic systems, the solution to Schrödinger's equation must satisfy Bloch's theorem. According to Bloch's theorem, for period systems such as crystalline structures, there exists a basis set of wavefunctions such that the wavefunctions may be written as

$$\psi_k(r) = \exp(ik.r)u_k(r) \quad \text{..... 10}$$

Where $u_k(r)$ has the same periodicity as the crystal structure. This formulation implies that the Schrödinger equation solved for each value of k independently. The k-space basis set, also known as reciprocal space, in which the k vector exists, naturally lends itself to describing periodic systems compared to using the spatial coordinates that define Euclidean space. Working with systems in k-space may be referred to as plane wave calculations as they exploit the plane-wave basis set $u_k(r)$ in Equation 3.11 denotes a plane wave functions. Many DFT calculations involve integrating functions of k vectors over the primitive cell of the system in k-space. The latter is also known as the Brillouin zone, and the selection of k values over which to perform integration in the Brillouin zone is a key parameter that must be specified in all DFT calculations. The periodicity of the $u_k(r)$ term in Equation 3.10 allows for it be further expanded in terms of a set of plane waves such that

$$u_k(r) = \sum_G G \exp(iG.r) \quad \text{..... 11}$$

Where the set of reciprocal-space vectors G is defined so that for any real space lattice vector, G = 2πm, where m is an integer value. Combining equation with Equation 3.10 and 3.11 gives

$$\psi_k = \sum_G cG + k \exp[i(k+G)r] \quad \text{..... 12}$$

Although this expression involves a summation over an infinite number of G vector values, the functions in Equation 3.12 can be interpreted as solutions of the Schrödinger equation containing kinetic energy, E = -h/2m |k +G|2. The infinite sum can therefore be truncated to include only solutions which have kinetic energies below a certain cutoff energy, allowing for the expression to be further reduced to

$$\psi_k = \sum_{|G+k|<G_{cut}} cG + k \exp[i(k+G)r] \quad \text{..... 13}$$

The cutoff energy G_{cut} determines which solutions are to be considered physically relevant to the problem, and is therefore another crucial parameter that must be carefully selected in all DFT implementations.

3.4.Pseudopotentials

The contribution of an atom's core electrons is often insignificant compared to that of the valence electrons. When modeling the physical interactions between atoms, core electrons often require very large energy cutoffs in plane wave calculations due to their small length scale oscillations. To address this inefficiency, the core electrons of atoms in a system can be approximated by pseudopotentials which consist of assigning an effective density to electrons under a certain radial cutoff. This approach simultaneously allows for the selection of a significantly lower energy cutoff, and for the size of the system to be reduced as only valence electrons is considered. A variety of pseudopotentials are available for DFT implementations, the three most common types being the ultrasoft pseudopotentials (US-PP) [51], the projected augmented wave (PAW) , and the norm- conserving pseudopotentials (NC-PP) [52].

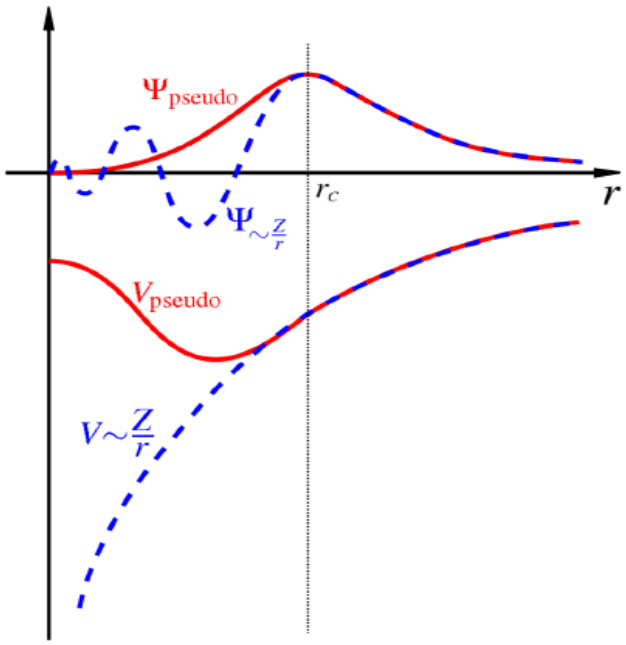

Figure 4: Comparison between coulomb potential and pseudopotential wavefunction. The curves with red color are pseudopotential curves and the curves with blue color are coulomb potential wavefunction curve. After the cut off radius r_c, both pseudopotential wavefunction and coulomb potential wavefunction match [53].

3.5.Software Package

3.5.1. Quantum ESPRESSO Software Package

We used the Quantum-ESPRESSO (QE) open-source software code to perform calculations presented in this thesis. QE is an integrated suite of computer codes for electronic structure calculations and materials modeling based on DFT, plane-wave basis set and pseudopotentials to

represent electron-ion interactions [54]. It is free software distributed under the terms of the GNU General Public License (GPL) [55]. The computational procedure of the QE code includes an iterative solution of the Kohn-Sham equations and optimized charge-density mixing routines. This includes the calculation of the Hellmann-Feynman forces acting on the atoms and the stresses on the unit cell. The total energy is optimized with respect to the positions of the atoms within a unit cell.

Inside this package, PWscf is the code we will use to perform total energy calculations. PWscf uses both NC-PP and US-PP, within DFT. For all DFT calculations, it should pay attention to two convergence issues. The first is energy cutoffs, which is the cutoff for the wave-function expansion. The second is number of k -points, which measures how well your discrete grid has approximated the continuous integral. [56]

3.5.2. Vienna Ab-initio Simulation Package - VASP

VASP, which full name is Vienna Ab-initio Simulation Package, is a software package developed by the Hafner Group of the University of Vienna for the calculation of electronic structures, quantum mechanics and molecular dynamics simulation. We can use VASP to obtain the electronic states and energies of the system by approximating the Schrödinger equation. It can solve the Kohn-Sham equation within the framework of the density DFT and is also possible to solve Hartree-Fock (HF) approximation.[57]

3.5.3. Visualization for Electronic and Structural Analysis -VESTA

Visualization for Electronic and Structural Analysis (VESTA) has been used to visualize both three-dimensional visualization of crystal structures and volumetric data in multiple windows with tabs. VESTA represents crystal structures by ball-and-stick, space-filling, polyhedral, wireframe, ball and stick, dot-surface and thermal-ellipsoid models. A variety of crystal-chemical information is extractable from fractional coordinates, occupancies and oxidation states of sites. It supports multiple windows, each of which may have multiple tabs assigned to graphics pages; two or more pages are switchable by clicking tabs with a mouse. Data and settings to reproduce the display of each page are saved in a small text file,*.vesta, with the VESTA format. It is highly scalable, enabling us to deal with practically unlimited numbers of objects such as atoms, bonds, coordination polyhedra and polygons on isosurfaces so long as memory capacity is enough. Objects can be rotated, scaled and translated fast in three dimensions [58]. The copper sulfide surface plane constructed and visualized in this work is by the VESTA software package

3.5.4. MATERIALS STUDIO

Materials Studio (MS) was employed to build molecular models, run classical simulations or perform quantum mechanical calculations. MS package contains many different modeling approaches and this is reflected in the diversity of the articles. The client (user interface) was made available under the Windows operating system (as opposed to, for example, UNIX or Linux), thus giving access of the software to a wider group of people (at least at that time), in particular in the R&D departments of major chemicals companies.[59]

This software can be used to determine the lattice parameters and electronic structure of material using quantum mechanical methods. In this software would examine the adsorption of molecule (OCHO, CO, COOH) on CuS plane surface. The surface was created from the optimized bulk CuS using Material Studio.

3.6. The PWscf method

As described in the second chapter, the set of Kohn-Sham equations is strongly non-linear and one has to adopt an iterative method in order to solve it.

The PWscf method implements an iterative approach to reach self-consistency, using at each step iterative diagonalization techniques, in the framework of the plane wave pseudopotential method. The procedure followed to do the self-consistent calculation is: one first makes a trial guess for the wave functions of all electrons and calculate its effective Kohn-Sham potential, V_{KS}. With this effective potential the Kohn-Sham equation is solved to get a new wave function. As shown in figure 6, a new V_{KS} is calculated, and so on. The procedure is terminated when the charge density does not vary much anymore. At this point self-consistency is reached, meaning that the wave function and the effective potential are self-consistent with each other, i.e. the wave functions correspond to those one would get from solving the Schrodinger equations with that potential. Both norm-conserving and ultrasoft pseudopotentials are implemented in the PWscf method.

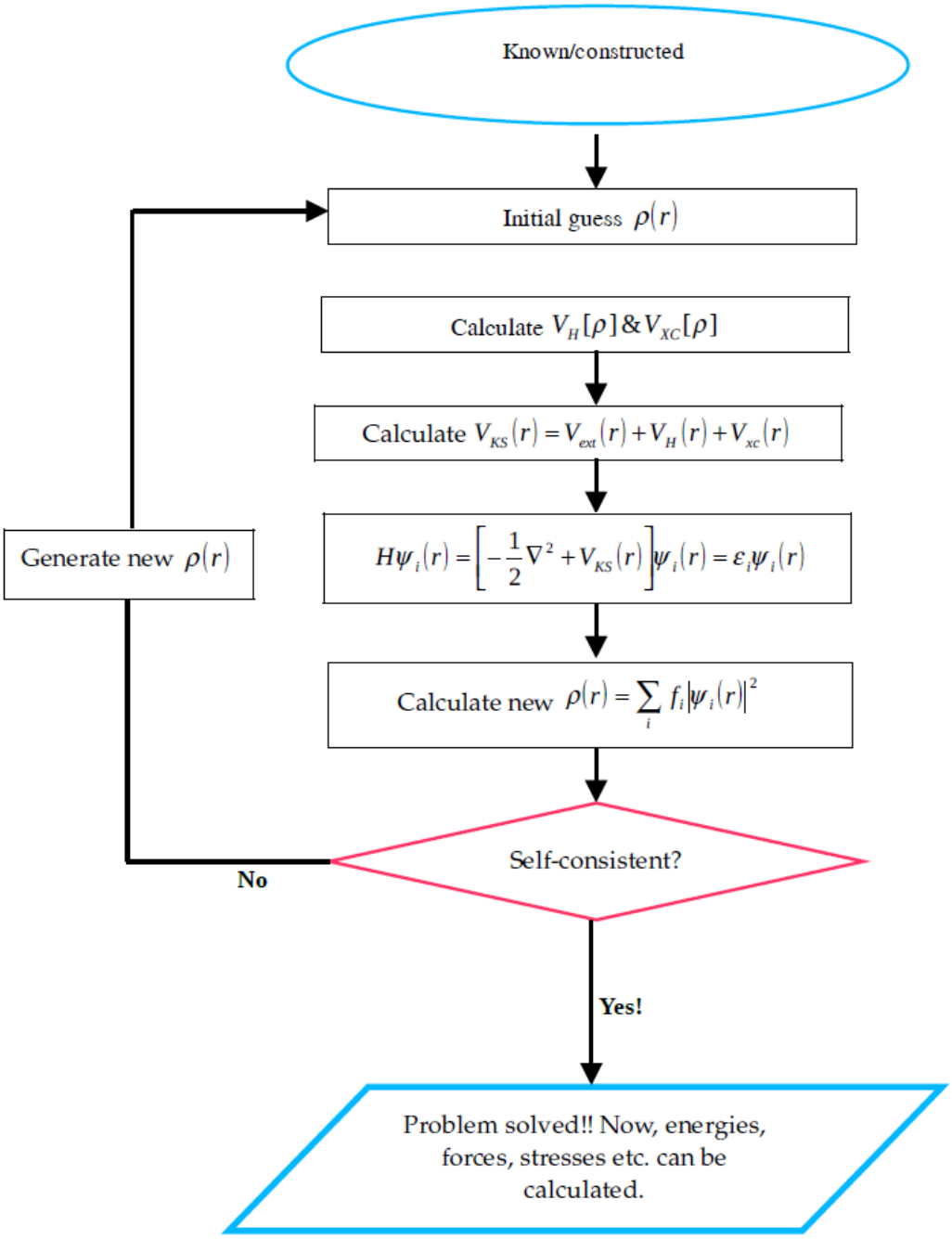

Figure 5. Calculation of the Kohn-sham ground state

3.6.1. Input File for a Simple PWscf Calculation

The input file for PWscf is constructed in a number of NAMELISTS and INPUT_CARDS. The use of NAMELISTS allows specifying the value of an input variable only when it is needed and to define default values for most variables that need not be specified. They are read in specific order and are ignored if not required. Three NAMELISTS are mandatory in PWscf. The first is &CONTROL which consists of the input variable that control the flux of the calculation and the amount of input/output on disk and on the screen. Input variables specifying the systems under consideration are listed in &SYSTEM. The third mandatory NAMELIST is &ELECTRONS, which contains the input variables that control the algorithms used to reach the self-consistent solution of the Kohn-Sham equations for the electrons.

INPUT_CARDS on the other hand are used to provide input data that are always needed and would be boring to specify with the variable_name = variable_value syntax used by NAMELISTS. Similarly, there are three mandatory INPUT_CARDS. The name, mass, and pseudopotential used for each atomic species present in the system are specified in ATOMIC_SPECIES. ATOMIC_POSITIONS is where the type and coordinates of each atom in the unit cell are specified. K_POINTS is the last mandatory INPUT_CARD used for the Brillouin zone integration.

3.7. Gibbs free energy Calculations

The free energy of adsorption was corrected from the electronic energy with zero point energy and entropy contributions estimated using ideal gas approximation and the harmonic approximation. These are used for molecules and adsorbates calculation respectively [60]. It is true even at a temperature arbitrarily close to absolute zero, since the lowest vibrational energy level for any bound vibration is *not* zero. Within the harmonic oscillator approximation, the energy of the lowest vibrational level can be determined from as $\frac{1}{2}h\nu$ where h is Planck's constant (6.6261×10^{-34} J s) and h is the vibrational frequency. The sum of all of these energies over all molecular vibrations defines the zero-point vibrational energy (ZPE). We define the internal energy at 0 K for a molecule as

$$U_o = E_{elec} + \sum_{i}^{modes} \frac{1}{2} h\nu_i \quad \text{.....14}$$

Where, E_{elec} is the energy for the stationary point on the Born–Oppenheimer potential energy surface. Vibrational contributions to the enthalpy and entropy of adsorbed species can also be obtained using the calculated vibrational frequencies [60].

$$\int_0^{298} Cv dT = \frac{h\nu}{e^{\frac{h\nu}{k_B T}-1}} \quad \text{.....15}$$

$$S = k_B \sum_i^{harmDOF} \left[\frac{h\nu}{k_B T\left(e^{h\nu/k_B T}-1\right)} - \ln\left(1-e^{-h\nu/k_B T}\right) \right] \quad \text{.....16}$$

Where, K_B is Boltzman constant $=1.38\text{x}10^{-23}\text{JK}^{-1}$

The free energy of each adsorbed species can be obtained by correcting the calculated electronic energies using the following method

$$\Delta G = \Delta H - T\Delta S = \Delta E_{DFT} + \Delta ZPE + \int_0^{298} C_v dT - T\Delta S \quad \text{.....17}$$

Where ΔE_{DFT} is the DFT optimized energy of the adsorbed intermediate

3.8. Computational Hydrogen Electrode (CHE) model

The computational hydrogen electrode (CHE) model suggested by Nørskov *etal ,2004,* which is coupled with energetics from DFT calculations to account for the chemical potential of proton–electron pairs without explicit calculation of their free energy. The CHE reference takes advantage of the equivalence of chemical potentials of the proton–electron pair and a hydrogen molecule at the reference relative hydrogen electrode (RHE) potential [13] at any pH value. It is used to calculate the free energy of adsorbates and reaction intermediates. In this model, the free energy change for each reaction step that involves an electron-proton pair transfer at 0 V (RHE) is calculated using the definition that the chemical potential of an electron-proton pair, i.e. $\mu(H^+ + e^-)$, is equal to that of one-half of hydrogen in the gas phase at standard pressure, i.e. $\frac{1}{2}\mu(H_2(g))$ [18].

$$H^+ + e^- \leftrightarrow H_2(g) \quad \text{..... 18}$$

The chemical potential of the proton–electron pair can then be calculated at this potential using DFT and statistical mechanics relationships to determine the free energy of the hydrogen gas molecule.

The variance of the proton–electron pair free energy with potential is simply determined using the linear free energy dependence of the electron energy on potential. At potentials different from 0 V (RHE), the chemical potential of the electron is shifted by – eU where e is the elementary charge and U is the electrode potential (RHE) respectively [27]. The total chemical potential of a proton–electron pair is written as follows

$$\mu(H^+) + \mu(e^-) = \frac{1}{2}\mu(H_2(g)) - eU \quad \text{.....19}$$

The free energy change for a general electroreduction reaction (surface bound species are denoted by a *)

$A^* + H^+ + e^- \Leftrightarrow AH^*$ 20

is those as follows

$\Delta G = G(AH^*) - G(A^*) - [\frac{1}{2}G(H_2) - eU]$ 21

Equation (3.21) is used to evaluate the potential-dependent reaction free energy for elementary CO2 reduction steps on the different surface, with DFT methods and statistical mechanics relationships used to determine the individual species free energies [13].

3.9. Adsorption Energy

Adsorption processes involve the interaction of one or more molecules with a surface, and one of the fundamental characteristics of the process is the adsorption energy. The adsorption energy is a criterion to determine the stability of the adsorption.

The adsorption energy is the difference between the energy of the products and the reactants. Negative adsorption energy indicates the products are more stable and hence molecule is likely to adsorb on the surface, corresponding to an exothermic process. The most negative energy and large adsorption indicates the most favored (stable structure) species or adsorption site. A positive energy suggests that adsorption on the surface is unlikely. [61]

$$E_{ads} = E_{Surface+Species} - E_{Surface} - E_{Species} \quad \text{.....22}$$

where $E_{Surface+species}$ is the total calculated electronic energy of the Surface and species of system in the equilibrium state, $E_{Surface}$ and $E_{Species}$ are the total electronic energies of slab (clean surface) and species (free molecule), respectively

Chapter Four

4. Results and Discussions

4.1. Computational detail

This work was based on DFT calculations with CHE model, used to calculate free energy of intermediate reaction and provided an explanation of the optimized structure of material, reaction path of the products formed, including H_2, CO and HCOOH it is relevant to reaction surface. Calculations using DFT have become a powerful tool for investigating catalytic reaction paths and processes by considering individual elementary reaction steps, and have helped identify new and improved catalysts. [9] [13]

In the calculations periodic plane wave DFT as implemented in Quantum Espresso program package and VASP software with the generalized gradient approximation (GGA) of Perdew–Burke– Ernzerh of (PBE) exchange correlation functional[50] and employing ultrasoft pseudopotentials[51]use for electron-ion core interaction were used. The integrations over the Brillouin zone were performed through the point sampling technique of Monkhorst and Pack [62] with k-points in the relevant irreducible wedge. This chapter focuses on study and investigate optimized structure of bulk copper sulfide, convergence analysis, optimized pristine CuS (001) surface structure, proposed elementary reaction path, calculate adsorbate energy and free reaction energy of configuration intermediate species to produce formic acid and carbon monoxide.

4.2. Electronic structure calculations and optimization of bulk CuS

4.2.1. Analysis of Kinetic energy cutoff, charge density cutoff and K-points grid

Convergence test is performed to obtain the converged cutoff energy, charge density cutoff and K-points for testing the convergence of total energy with each parameters calculation to get the minimum energy, which is going to be used to make further calculation on CuS materials. The result is shown in figure 7. Calculation convergence test for kinetic energy cutoff plan wave (ecutwfc) and charge density cutoff which is used for total electronic energies convergence using self-consistent field (scf) of a plane wave basis was performed to get a true representation of the CuS material. These kinetic energy and charge density cut off are the parameter in theory which control the accuracy of description of a system and is a property of the pseudopotential used in determining initial optimized structure. For this calculation using convergence tests, the Kohn-Sham wave functions were expressed with plane wave basis set cut-off energy of 60 Ry and a charge density cut-off of 450 Ry and the criterion for self-consistent field convergence energy threshold defining geometric optimization with variable unit cell coordinates (vc_relax calculation) of the electron density for bulk

structure was set to 10^{-8} Ry with exchange-correlation functional PBE and ultrasoft pseudopotentials and also, Monkhorst-Pack [63] Brillouin zone sampling was carried out at 12 x 12 x 3 k- point was used for the bulk and 3x3x1 for the slab (because of vacuum introduction). This value was used throughout all calculations, both in the bulk and slab (surface) models. It was chosen as it is the least converged point on the curve which will make the calculations computationally less expensive. Visualization of structures was done using the XCrySDen and VESTA software package.

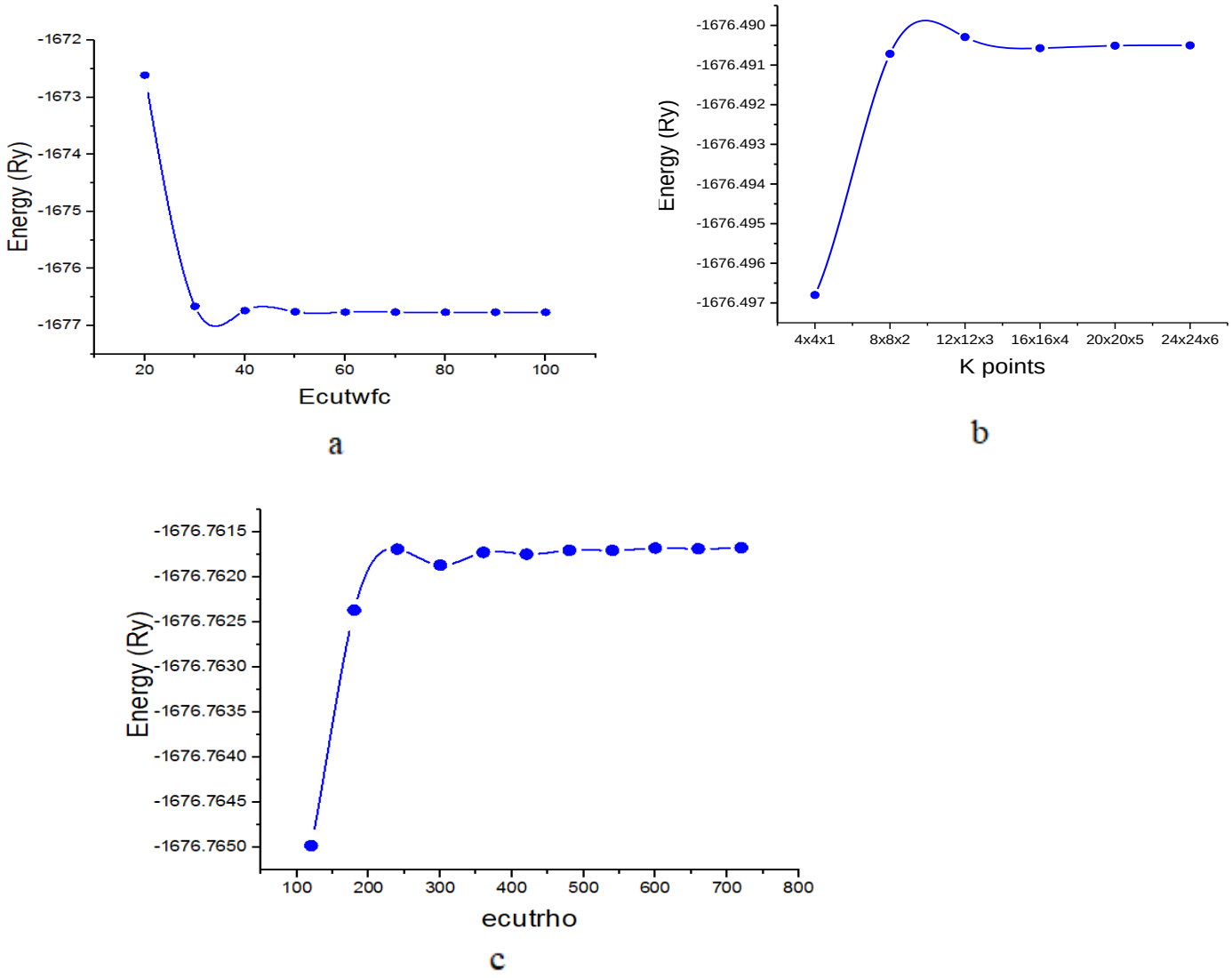

Figure 6 Convergence test for optimized bulk CuS. (a) Total energy vs Kinetic energy cutoff, (b) Total energy vs K points and (c) Total energy vs charge density cut-off energy

Bulk CuS is a hexagonal unit cell, the cell parameters and interatomic bond distance and angles were characterized by performing full geometry optimization calculations from its initial crystal structure

parameters of a=3.7574 Å, c = 16.27629 Å are in good agreement with the experimental ones (a = 3.794 Å and c = 16.341 Å) [64] . This relaxed structure is used to construct models of CuS (001) surfaces. The optimized structure(s) and structural parameters are respectively shown in Figure 9 and Table 4.

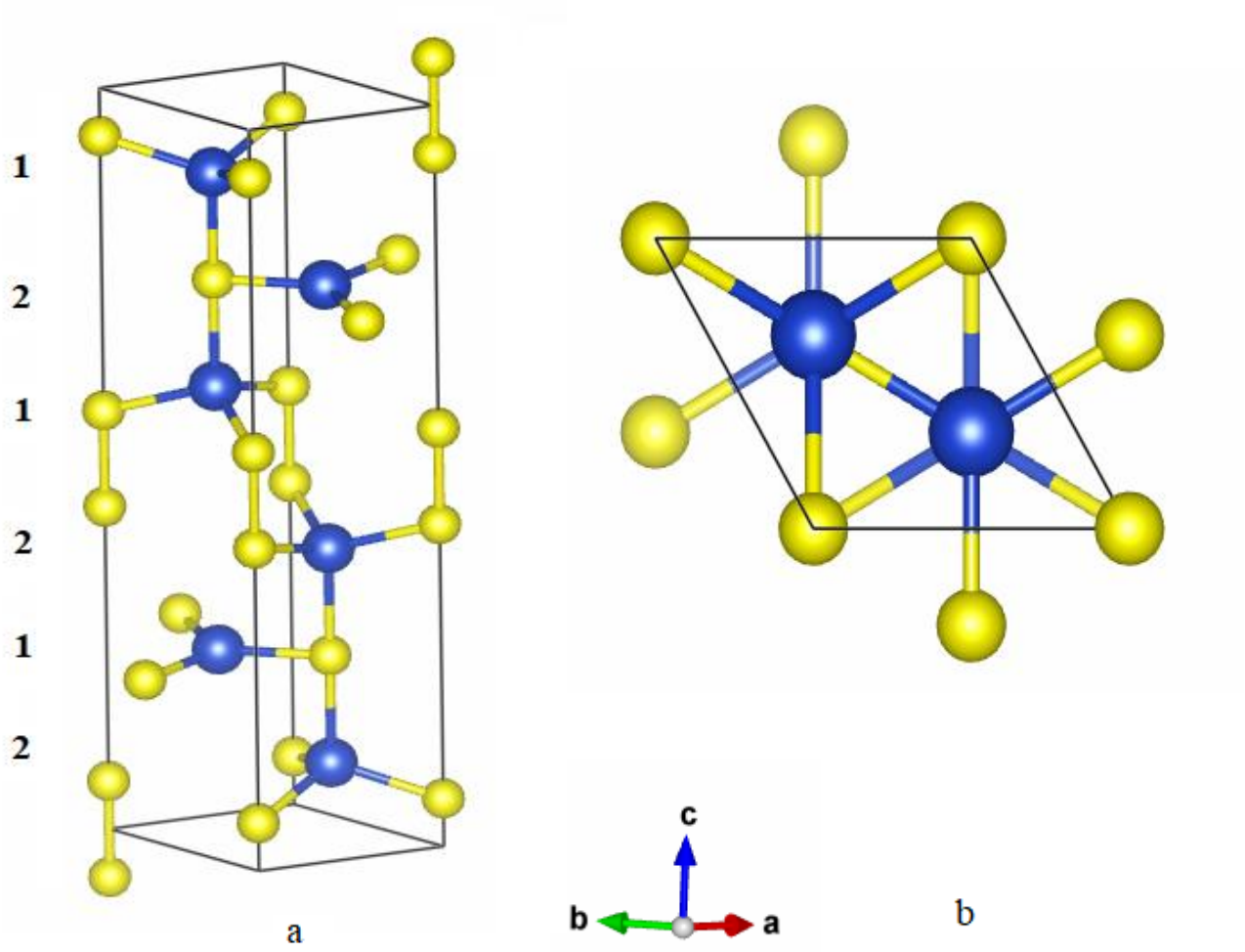

Figure 7 Optimized Covellite hexagonal unit cell (CuS). (a) side view (b) top view . 1 and 2 represent Cu in tetrahedral and triangular position. Blue and yellow spheres are copper and sulfur atoms, respectively

Table 3 DFT optimized bulk CuS crystal structure parameters and comparison with experimental parameters

Covellite	Space group	Lattice parameter (Á)	Experimental	This work
CuS	(P63/mmc)[65]	a=b c V c/a	3.796[65], 3.7938[43], 3.8073[38] 16.382[65],16.341[43],16.523[38] 204.4[65] ,202.5[43] 4.316[65],	3.75744 Å 16.27629 Å 199.0074 Å^3 4.33175
Triangle		Cu(l)-S(l)x 3	2.1915[65], 2.190[43]	2.26804 Å
Tetrahedron		Cu(2) - S(l) Cu(2) - S(2) x 3 S(2) -S(2)	2.339[65], 2.331[43] 2.305[65], 2.305[43], 2.086[65], 2.071[43], 2.07[38]	2.35258 Å 2.16934 Å 2.10941 Å

The calculated results shown in table 3 include lattice parameter, tetrahedral, triangular bond length and angle is a good approximation between this work and preceding study [34][39][58]. This structure is essential for the calculation of surface structure. The parameters of bulk CuS such as cut off energy, charge density cutoff of the bulk consider in surface calculation.

4.3. Calculation Optimized of Pristine CuS (001) Surface

Surface energy of CuS with various miller plane index surface of (001), (100), (020), and (102) are 0.160, 0.404, 0.420 and 0.649 Jm^{-2} respectively. Among these surfaces, CuS (001) surface has the smallest surface energy (0.16 J m^{-2}). This smallest surface energy determines those CuS (001) surfaces are the most stable surface under the pressure (10^{-3} atm) and temperature (300 K) conditions. Surface CuS (001) was chosen is the most thermodynamically stable surface of the hexagonal crystallographic structure [38][64] .

Structure of optimized CuS (001) surface calculations was performed via periodic plane-wave DFT using the Quantum Espresso software Package the plane waves basis set was used to perform relaxation calculation using the parameter' relax'. To calculate the pristine structure of surface take the lattice parameter, energy cutoff (60 Ry), charge density cutoff energy (450 Ry) and atomic coordinates of the bulk, and then cleave the surface of the optimized bulk using material studio and VASP software package on (001) cleave plane. The slab CuS (001) constructed with 4 atomic layer and 72 atoms (Cu=36 and S=36).The vacuum space separated by 15 Å in the direction perpendicular to the surface plane. At such a space avoids unphysical image interactions among the neighboring layers. During geometry optimization we would fix the bottom most two atomic layers and allow the renaming atoms to relax freely.

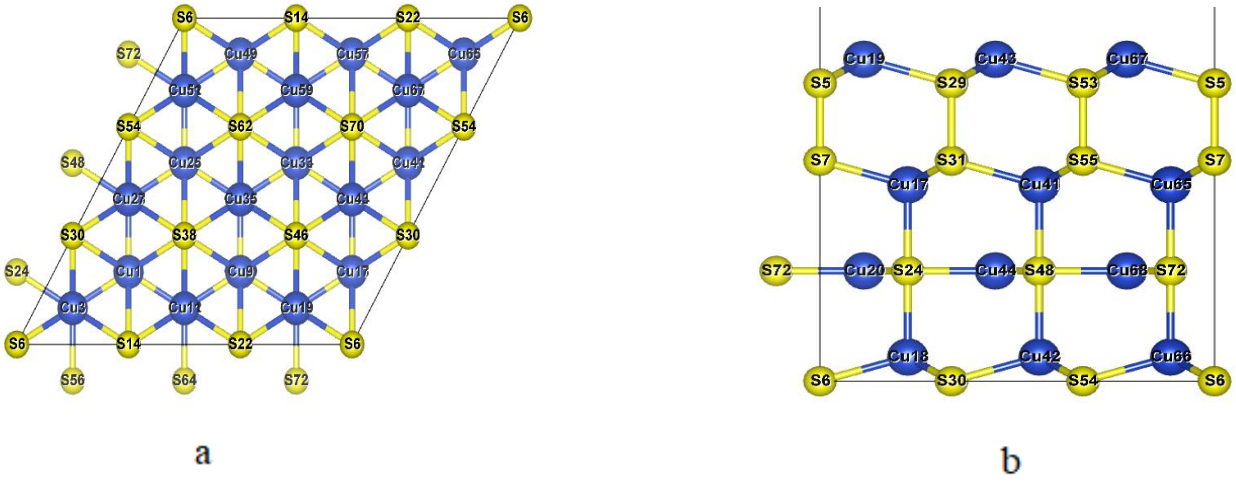

Figure 8. The computational models of pristine CuS (001) surface optimized structure. (a)Top and (b) Side view

During the calculations, the structure of the bottom two layers were fixed at the theoretical bulk positions, whereas the top two layers and the intermediate were allowed to relax and all the other structural parameters were optimized so as to minimize the total energy of the system. Table 4 summarizes layer and termination of copper and sulfur atom. It is noted that during the cleaving process the exposed atoms have lower coordination than those in the bulk structure inducing a certain degree of polarization in the slab. This slab models are symmetric showing that the termination of the top and bottom of the slab is the same. Then, the polarization is basically cancelled by an equal and opposite effect on the other side of the slab. The atomic internal coordinates of all surfaces are relaxed to maintain this cancelling out effect.

Table 4 Atoms (and their IDs) of the CuS (0 0 1) surface within the VESTA showing layers they occupy and the layer's termination.

Termination	Layer	Atom	ID
S-Cu- S-Cu- S-Cu- S	First	S, S, S, Cu, Cu, Cu	5, 29,53,19, 43,67
S-Cu- S-Cu- S-Cu- S	Second	S, S, S, Cu, Cu, Cu	7, 31, 55, 17, 41, 65
S-Cu- S-Cu- S-Cu- S	Third	S, S, S, Cu, Cu, Cu	24, 48, 72, 20, 44, 68
S-Cu- S-Cu- S-Cu- S	Fourth	S, S, S, Cu, Cu, Cu	6, 30, 54, 18, 42, 66

4.4. Optimized structure of Clean CuS (001) surface with Intermediate

In this section, we determined the optimized structure of CuS (001) with adsorbate species *H, *OCHO, *COOH,*CO using DFT study with VASP and material Studio package. As shown here the geometry optimized configuration formed to various possible combinations for the adsorption sites of H, OCHO, COOH, and CO on CuS (001) the surface. We then compare the calculated activation energies of these adsorption configurations and choose the lowest total energy (the most stable) that is favourable for the desired products.

Atom species colors are Oxygen, Hydrogen, Carbon, Sulfur and Copper atoms are red, white, gray, blue and yellow respectively.

a b

Figure 9 Geometry optimization plot of H adsorbed on the CuS (001) surface (a) View along y- axis (b) View along z- axis

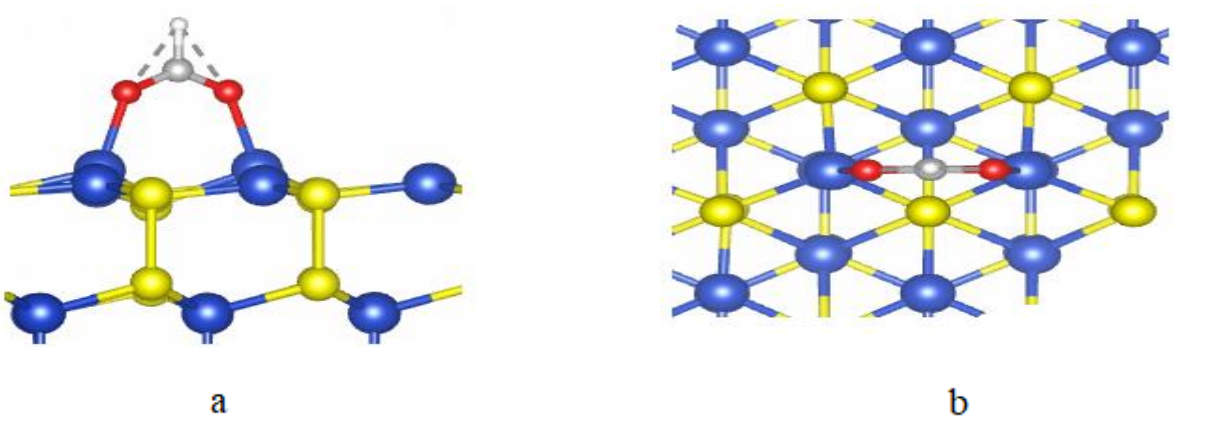

Figure 10. Geometry optimization plot of OCHO adsorbed on the CuS (001) surface (a) View along y- axis (b) View along z- axis

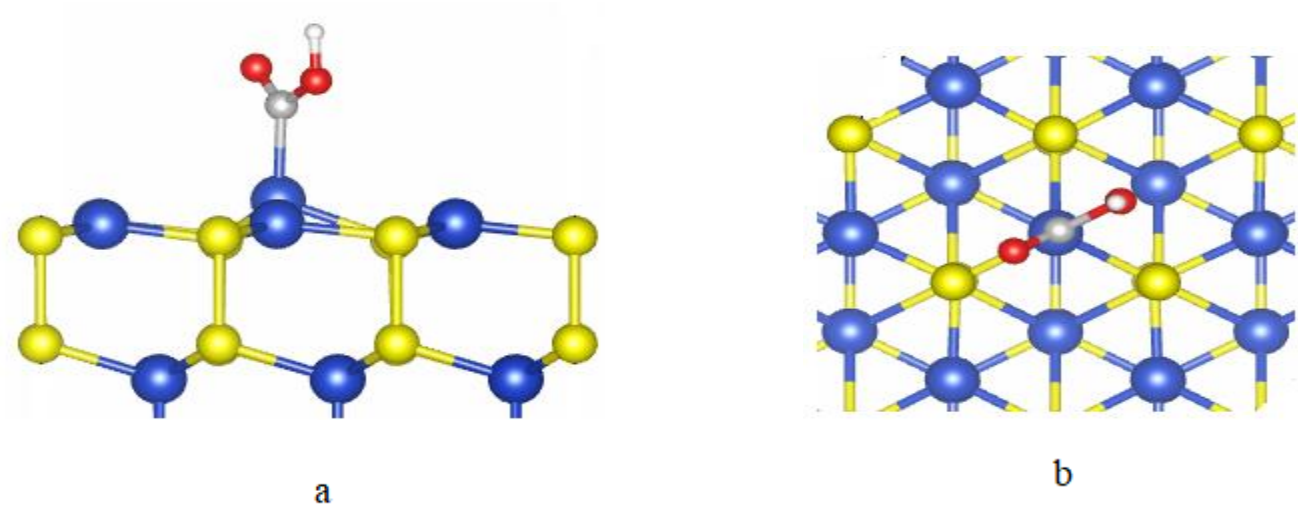

Figure 11. Geometry optimization plot of COOH-Cu adsorbed on the CuS (001) surface (a) View along y- axis (b) View along z- axis

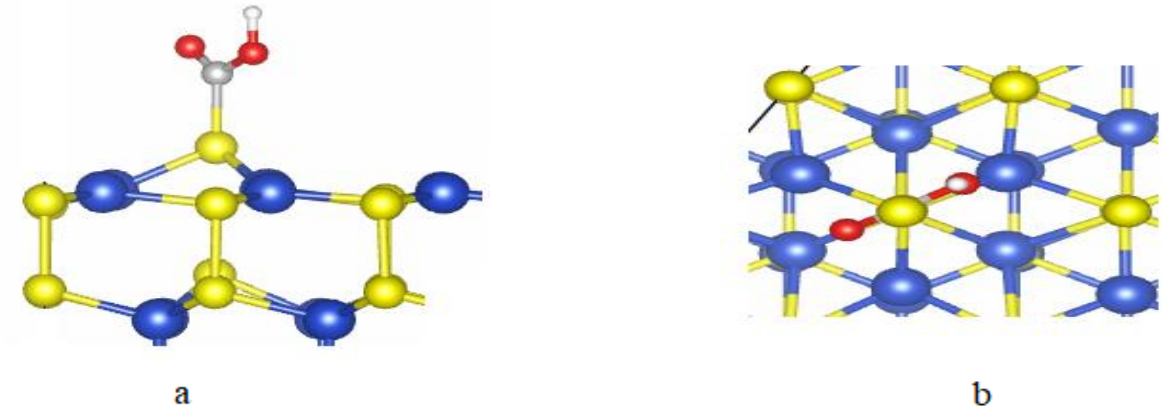

Figure 12. Geometry optimization plot of COOH-S adsorbed on the CuS (001) surface (a) View along y- axis (b) View along z- axis

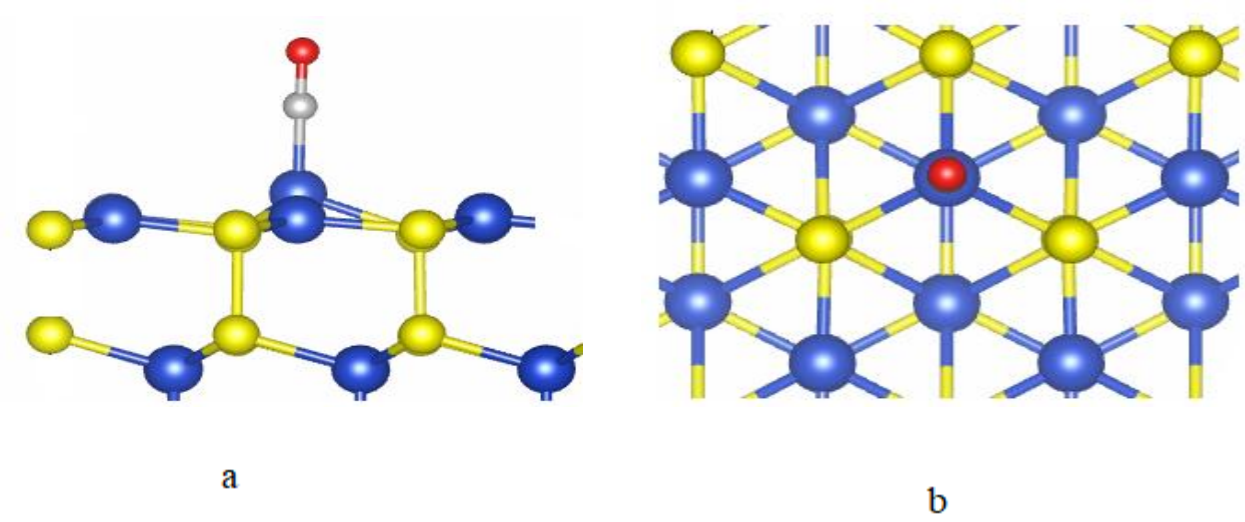

Figure 13. Geometry optimization plot of CO adsorbed on the CuS (001) surface (a) View along y-axis (b) View along z- axis.

4.5.ECR reaction to Formic acid and Carbon monoxide on slab CuS (001)

4.5.1. Reaction pathways for key intermediates

Based on the previous studies by Nie et al. and Peterson et al., two proposed reaction paths for CO_2 electroreduction on CuS are considered and summarized in Figure 15 [66].Two separate products of CO_2 electroreduction result from the proposed pathways: HCOOH and CO.

Both reactions path predicts the formation of HCOOH and CO on surface CuS (001) of CO2 electroreduction proceed via *OCHO and *COOH intermediates reaction path. Reaction $CO_2 + H^+ + e^-$ on the surface of CuS (001) catalyst tends to be protonated/ reduced at the C-position results in the production of formate (*OCHO). Alternatively, $CO_2+H^++e^-$ on the surface of CuS (001) catalyst tends to be protonated/reduced at an O-position which results in the production of a *COOH intermediate that can be further reduced to *CO. If the *CO is weakly bound to the CuS (001) catalyst, further reduction of this intermediate leads to it's desorption as CO product. CuS was found to catalyze the conversion of CO_2 into HCOOH and CO. Figure 14 shows the two most proposed reaction pathways in the formation of HCOOH and CO from the electrochemical conversion of CO_2.

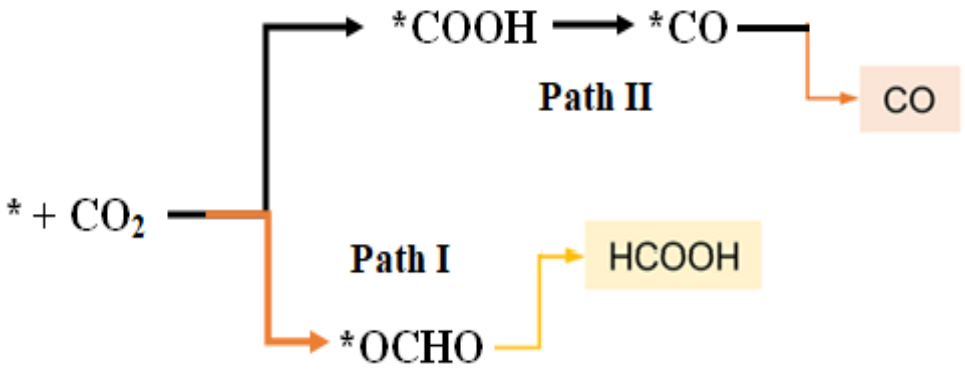

Figure 14. The proposed reduction reaction paths of CO_2 to HCOOH and CO on CuS (001). The proton and electron reactants and water molecule products are not included in the reaction scheme.

The proposed carbondioxide reductions have two elementary reaction pathways for H, CO and HCOOH productions on CuS (001) surface are shown in Figure 14 Path I through a *OCHO intermediate and path II through a *COOH intermediate, these steps involve CO_2 reduction to *COOH and further reduction of *COOH to *CO. The reactions step for the ERC of CO_2 to HCOOH, CO, and the computing HER are using the following reaction step

Formic acid:

$* + CO_2 + H^+ + e^- \leftrightarrow *OCHO$ .....(23)

$*OCHO + H^+ + e^- \leftrightarrow HCOOH$ .....(24)

Carbon monoxide:

$* + CO_2 + H^+ + e^- \leftrightarrow *COOH$ .....(25)

$*COOH + H^+ + e^- \leftrightarrow *CO + H_2O$ .....(26)

$*CO \leftrightarrow CO + H_2O$ .....(27)

Hydrogen:

$\mathbf{* + H^+ + e^- \leftrightarrow H*}$ .....(28)

$H* + H^+ + e^- \leftrightarrow H_2$ .....(29)

Here below we calculated the adsorbed energy of optimized structure intermediate *H, *OCHO, and * COOH, and *CO on a CuS surface and pristine surface energy at CO_2 reduction.

Table 5 Complex (CuS (001) + adsorbate), slab CuS (001) and intermediate (adsorbate) energy obtained from the DFT calculation (using VASP software package).Where an asterisk (*) designates that the intermediate (*H, *OCHO, *CO, *COOH) was adsorbed on the catalytic surface.

	***H**	***CO**	***OCHO**	***COOH_Cu**	***COOH_S**
$E_{Complex}$ (eV)	-309.27	-321.21	-332.67	-331.54	-331.13
$E_{surface(CuS001)}$ (eV)	-305.49	-305.49	-305.49	-305.49	-305.49
$E_{intermediate}$ (eV)	-3.78	-15.73	-27.18	-26.06	-25.64

4.6. Detail calculation of activation energy of CO_2 reduction

Density functional theory (DFT) calculations based on a computational hydrogen electrode(CHE) model provides the activation free energies [9] of the CO_2 reduction intermediates in electrochemical reaction pathways figure 14 .The CHE model defines that the free energy of a proton/electron ($H^+ + e^-$) is equal to half of the free energy of a gas-phase H_2. At 298 K and 1 atm, the Gibbs free energy (G) of intermediate *H, *OCHO, *COOH, *CO was calculated according to Eq. (**14-16**)

a) Zero-point energy, enthalpy and entropies correction of intetmediate

In this section, firstly calculate vibrational frequency each intermediate using VASP software package. Secondly, based on standard computational method[60] calculate energy correction to Zero-point energies, entropies, and heat capacities lastly, compute the total energy obtained from the DFT calculation . Gas phase molecules, CO_2 and H_2, were treated as ideal gas, while adsorbates were treated using the harmonic approximation.

Table 6 Contributions to the adsorbate free energy from the zero-point energy correction, enthalpic temperature correction, entropy, and the total free energy correction, respectively. All values are given in eV

Intermediate/ adsorbate	ZPE	$\int C_v dT$	-TΔS	ZPE+ $\int C_v dT$ -TS
***CO**	0.19	0.08	-0.2	0.07
***COOH$_{-Cu}$**	0.37	0.12	-0.35	0.14
***COOH$_{-S}$**	0.63	0.11	-0.29	0.45
***OCHO**	0.61	0.1	-0.21	0.5
***H**	0.22	0.01	-0.02	0.21

The computational hydrogen electrode model (CHE) was employed to calculate the change in Gibbs free energy, ΔG, along the reaction path Figure 14. Electronic energy determined using density functional theory (DFT) calculations were carried out with the Vienna Ab Initio Simulation package (VASP). Electronic energy of complex (surface + intermediate) structure, clean surface CuS (001), and adsorbate species (*H, *OCHO, *COOH, *CO) is given in table 6 above.

b) Electronic energy Zero-point energy, enthalpy and entropies correction of Gas phase molecules

Table 7 Electronic energy, Zero-point energy correction, enthalpy correction, and entropy correction for free gaseous molecules with their partial pressure of 101325 Pa and temperature 298 K [19],[67]. All values are given in eV.

Molecule	E_E	ZPE	$\int C_v dT$	-TΔS	ZPE+ $\int C_v dT$ -TΔS
CO	-14.79	0.14	0.12	-0.6	-0.34
H_2	-6.76	0.27	0.06	-0.4	-0.07
HCOOH	-29.93	0.89	0.11	-1.05	-0.05
CO_2	-22.99	0.31	0.1	-0.66	-0.25
H_2O	-14.027	0.58	0.1	-0.65	0.03

The Gibbs free energy, ΔG, is the energy difference between the energy minimum and the transition state of the reaction. It is therefore of interest to determine the activation barriers of reactions. The activation barriers and transition states associated with the reaction can then be obtained from the minimum energy pathway. Calculations of activation barrier energy of intermediate are using elementary reactions using, Eq. (17), Eq. (21) and Eq. (23-27) as shown below.

i. Calculation of hydrogen evolution reaction (HER)

The hydrogen evolution reaction (HER), requires a bound proton (H*) intermediate .The Gibbs free / activation barrier energy of formation for an intermediate *H based on reaction (28-29) is

$$\Delta G * H = \Delta G_{DFT*H} - 0.5\Delta G_{H}$$

$$= -3.58 - (-3.42)$$

$$= -0.16 \text{ eV}$$

Hydrogen production is a faster reaction with activation energy of -0.16 eV on CuS (001)

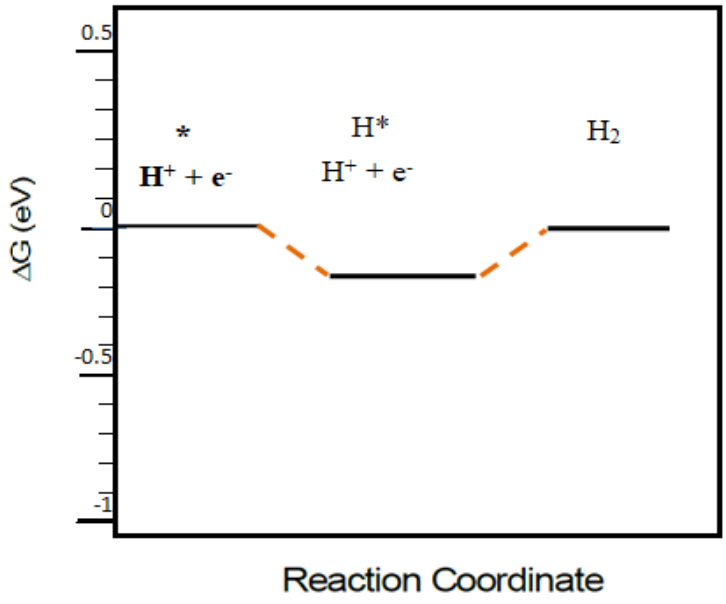

Figure 15 Relative free energy diagrams for reaction pathway through H* intermediate, at 0 V–RHE.

ii. Formic acid Production Pathway via *OCHO Intermediate

The Gibbs free energies of the dominant pathways for formate production on CuS (001) surfaces via *OCHO intermediates at zero potential are presented in Figure 16. Activation energy of formation an intermediate (ΔG_{*OCHO}) to formic acid is based on reaction (23) and reaction pathway I is calculated as

$$\Delta G(_{*OCHO}) = \Delta G_{DFT*OCHO} - \Delta G_{CO_2} - 0.5\Delta G_H)$$

= -26.685 – (-23.24-3.415)

= **-0.03 eV**

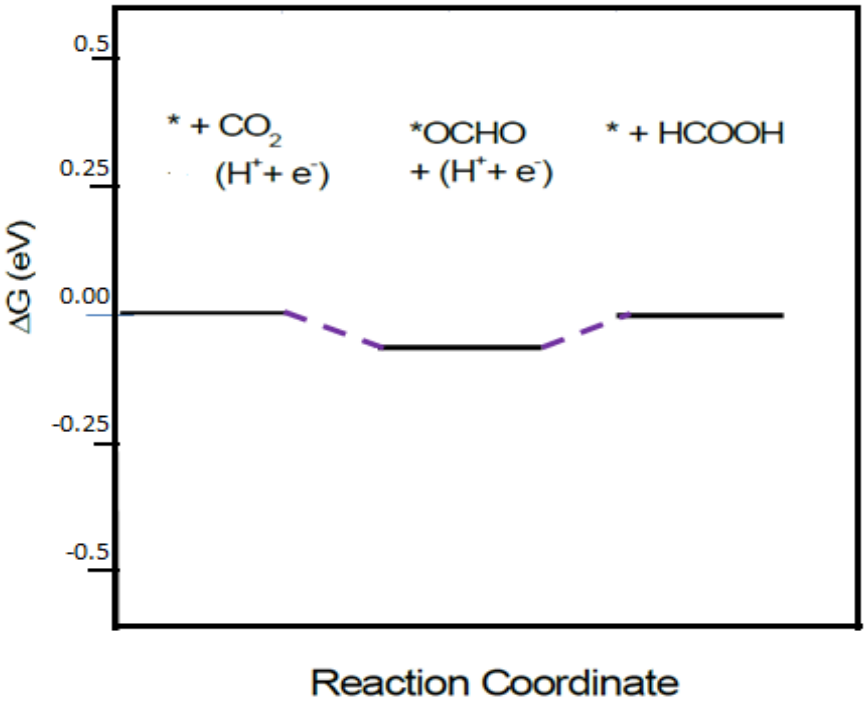

Figure 16 Relative free energy diagrams for reaction Pathway I through *OCHO intermediate, at 0 V–RHE.

iii. CO Production Pathway via *COOH Intermediate on CuS (001) surface.

a. COOH intermediate on Copper atom ($*COOH_{-Cu}$)

The free energies of the reaction mechanism for CO formation via $*COOH_{-Cu}$ intermediates at 0V on CuS (001) surface, with the last desorption step from *CO to CO (g), are presented in figure 17. At 0 V, the formation of $*COOH_{-Cu}$ intermediates is calculated as follows using reaction (25) and reaction pathway II,

$$\Delta G(*COOH_{-Cu}) = \Delta G_{DFT*COOH} - (\Delta G_{CO_2} + 0.5\Delta G_H)$$

=-25.92-(-23.24-3.42)

= 0.74 eV

Gibbs free /activation energy $*CO_{-Cu}$ intermediate (ΔG) for formation of carbon monoxide based on reaction (26) and pathway II figure 14, as follows

$$\Delta G*CO_{-Cu} = \Delta G_{DFT*CO} - \Delta G_{*COOH/cu} + \Delta G_{H_2O} - 0.5\Delta G_H$$

= -15.66 – (-25.92) + (-14.00) – (-3.42)

= -0.32 eV

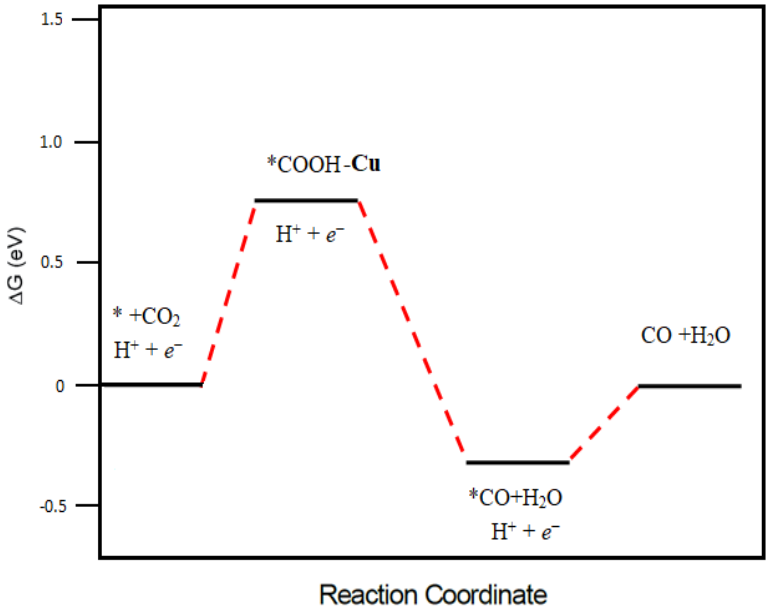

Figure17 Relative free energy diagrams for reaction Pathway II via $*COOH_{-Cu}$ and *CO intermediate, at 0 V–RHE

b. *COOH intermediate on Sulfur atom ($*COOH_{-S}$)

Gibbs free/ activation energy of formation for an intermediate $*COOH_{-S}$ (ΔG) is based on reaction (25) and path II figure 14, ΔG *COOH-S is

$$\Delta G(*COOH_{-S}) = \Delta G_{DFT*COOH} - (\Delta G_{CO_2} + 0.5\Delta G_H)$$

= -25.19- (-23.24 -3.42)

= 1.47 eV

Change Gibbs free /activation energy of formation of intermediate *CO_{-S} based on reaction step (25) and path II, ΔG *CO_{-S} is

$$\Delta G*CO_{-S} = \Delta G_{DFT*CO} - \Delta G_{*COOH/a} + \Delta G_{H_2O} - 0.5\Delta G_H$$

= -15.66 – (-25.19) + (-14.00) – (-3.42)

= -1.05 eV

Calculated activation energy of conversion *COOH to *CO is -1.05 eV.

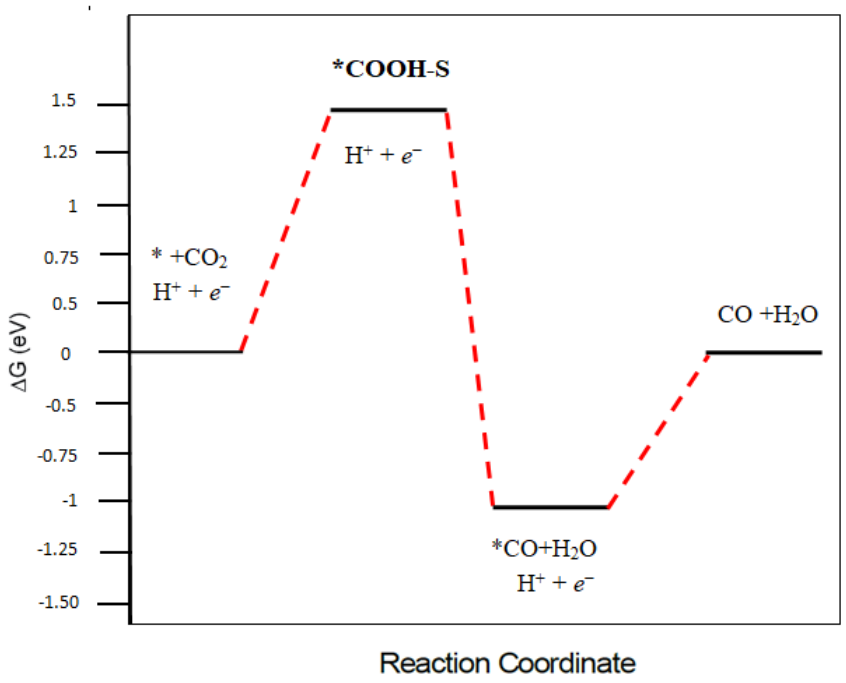

Figure 18 Relative free energy diagrams for reaction Pathway II through *COOH-S and *CO-S intermediate, at 0 V–RHE

In table 8 calculated activation barrier energy of intermediate reaction *OCHO, *H, *$COOH_{Cu}$, *CO_S, *COOH-S, and *CO-S formation on CuS (001) surface are -0.03, -0.16, 0.74, -0.32, 1.47, and -1.05 eV respectively. From free energy of intermediate *OCHO (-0.03 eV) is small, this result showed that *OCHO intermediate is the most favourable intermediate and better selective catalyst toward formation of formic acid on CuS (001) surface.

Table 8 Summery of calculation Gibbs free/ activation barrier energy to the adsorbate including the zero-point energy correction, enthalpic temperature correction, entropy, and the total free energy correction, respectively based on harmonic vibrational free energy at 298.15 K. All values are given in eV.

Intermediate molecule	E_{DFT}	ZPE	$\int C_v dT$	-TΔS	ΔG
***H**	-0.40	0.09	-0.02	0.18	-0.16
***OCHO**	-0.81	0.17	-0.03	0.65	-0.03
***COOH-Cu**	0.314	-0.075	-0.01	0.51	0.74
***COOH-S**	0.730	0.185	-0.02	0.57	1.47
***CO-Cu**	-0.317	0.265	0.03	-0.30	-0.32
***CO-S**	-0.733	0.005	0.04	-0.36	-1.05

Free activation energy of intermediate *COOH-Cu is 0.74 eV. It is less than activation energy of intermediate *COOH-S (1.47 eV) .This result shows that *COOH-S adsorbate on sulfur atom is less selective for the Carbon monoxide production. This is because of the bond length between C-S (1.81051 Å) is less than C-Cu (1.94735 Å).

Table 9 Comparing results of activation energy of formation HCOOH in different catalytic surface

Surface	ΔG (eV)	Reference
CuS (001)	-0.03	This work
In (110)	-0.423	[67]
Zn (002)	-0.623	[67]
Pb(211)	-0.30	[29]
Ru (0001)	-0.76	[68]

Intermediate species *OCHO is formed with an absolute free energy barrier of 0.03eV on CuS (001) surface. From table 9 showed that free energy change of the intermediate with respect to the reactants in different surface such as CuS (001), Pb (211), In (110), Zn (002). Free energy change of the

intermediate (ΔG) is -0.03 eV, -0.30 eV, -0.423 eV, and -0.623 eV, respectively. In CuS (001) surface, free energy is smaller than the other surfaces hence easy reaction occurred than Pb (211) and In (110). This shows that the presence of sulfur weakens activation energy of *OCHO such that formation of *COOH toward CO is suppressed, while the formation of *OCHO toward formic acid is more favored [69].Our calculation indicate that CuS (001) catalysis is more energetically favorable for the HCOOH production than In (110) and Pb (002) surface catalysts. However *COOH-S activation barrier energy is indeed higher than that of COOH-Cu (1.47 eV vs 0.74 eV).This indicates that COOH-S less favorable in conversion of CO_2 in to CO. This result showed that CuS 001 surface highly selective to formic acid formation.

CHAPTER FIVE

5. Conclusion and Recommendation

In conclusion, the evaluated and calculated activation barrier energy for each intermediate using DFT with CHE model for electrochemical reduction of carbon dioxide into formic acid and carbon monoxide useful products. Optimized structural properties of bulk CuS and CuS (001) surface were studied using material studio and Vesta software. From DFT calculation using Gibbs free energy equations we obtained small activation energy on intermediate *OCHO is -0.03 eV this indicate that easier reaction occurred in the elementary reaction pathway $* + CO_2 + H^+ + e^- \leftrightarrow$ *OCHO. Moreover, calculation result predicts higher catalytic activity for CO_2 reduction on CuS (001) surface than on Pb (211) and In (110) surface with activation barrier energy -0.30 eV and -0.423 respectively. Hence, CuS (001) surface catalyst more favorable reaction and better selective to formic acid production. Activation barrier energy of *COOH_cu intermediate is 0.74 eV it is smaller than *COOH-S (1.47eV) intermediate. This shows that intermediate *COOH-Cu more favorable reaction for carbon monoxide formation.

The following points are recommended for further study:

In the present research, copper sulfide as a low-toxicity and emerging material, has broad prospects in the field of CO_2 reduction due to its unique structural and electrochemical properties. In the future, the heterostructures can be studied using Heyd-Scuseria-Ernzerhof (HSE06) hybrid functional approximation to get better electronic structure and properties, which therefore, will significantly improve their selectivity and activity of final products. Additional formation of larger hydrocarbons through C–C bond formation may occur along either path, though the formation of hydrocarbons is not considered in this study. Further studies are also recommended to chemical kinetics that affects the rate of chemical reactions need to be investigated. Finally, experimental works can be performed to validate the theoretical results.

References

[1] I. S. Kwon *et al.*, “Selective electrochemical reduction of carbon dioxide to formic acid using indium – zinc bimetallic,” pp. 22879–22883, 2019.

[2] A. R. T. Morrison *et al.*, “Modeling the Electrochemical Conversion of Carbon dioxide to Formic Acid or Formate at Elevated Pressures,” 2019.

[3] M. Jitaru, “Electrochemical carbon dioxide reduction - Fundamental and applied topics,” no. January 2007, 2015.

[4] F. Yu, P. Wei, Y. Yang, Y. Chen, L. Guo, and Z. Peng, “Nano Materials Science Material design at nano and atomic scale for electrocatalytic CO_2 reduction,” vol. 1, no. February, pp. 60–69, 2019.

[5] M. Loa, “Annual Mean Global Carbon Dioxide Growth Rates.” [Online]. Available: http://www.esrl.noaa.gov/gmd/ccgg/trends/gl_gr.html.

[6] V. A. Online, E. V Kondratenko, G. Mul, and J. Baltrusaitis, “Environmental Science,” pp. 3112–3135, 2013.

[7] S. Wang, “A Study of Carbon Dioxide Capture and Catalytic Conversion to Methane using a Ruthenium , ‘ Sodium Oxide ’ Dual Functional Material : Development , Performance and Characterizations,” 2018.

[8] I. Merino-garcia, J. Albo, J. Solla-gullón, V. Montiel, and A. Irabien, “Cu oxide / ZnO-based surfaces for a selective ethylene production from gas- phase CO_2 electroconversion,” *J. CO_2 Util.*, vol. 31, no. March, pp. 135–142, 2019.

[9] and E. S. Javed Hussain, Hannes Jonsson, “Calculations of product selectivity in electrochemical CO_2 reduction,” *ACS*, 2018.

[10] A. C. Guo *et al.*, “Electrochemical CO_2 Reduction to C1 Products on Single Nickel/ Cobalt/Iron doped Graphitic Carbon Nitride: a DFT Study,” *Chem pubsoc Eur.*, 2019.

[11] H. Zhou *et al.*, “Journal of Colloid and Interface Science Recent advances in different-dimension electrocatalysts for carbon dioxide reduction,” vol. 550, no. May 2018, pp. 17–47, 2019.

[12] L. Ou, “Chemical and electrochemical hydrogenation of CO_2 to hydrocarbons on Cu single crystal surfaces : insights into the mechanism and selectivity from,” *RSC Adv.*, vol. 5, pp. 57361–57371, 2015.

[13] X. Nie, W. Luo, M. J. Janik, and A. Asthagiri, “Reaction mechanisms of CO_2 electrochemical reduction on Cu (1 1 1) determined with density functional theory,” *J. Catal.*, vol. 312, pp. 108–122, 2014.

[14] A. Boulamanti, G. Harrison, and E. Tzimas, “ScienceDirect Formic acid synthesis using CO_2 as raw material : Techno-economic and environmental evaluation and market potential,” vol. 1, 2016.

[15] Y. Chen *et al.*, “Nano Materials Science Recent advances in the utilization of copper sul fi de compounds for electrochemical CO_2 reduction,” no. August, 2019.

[16] R. Garc, F. Dattila, T. Shinagawa, and A. J. Mart, “Origin of the Selective Electroreduction of Carbon Dioxide to,” 2018.

[17] Y. Deng *et al.*, “On the Role of Sulfur for the Selective Electrochemical Reduction of CO 2 to Formate on CuS x Catalysts,” *ACS Appl. Mater. Interfaces*, vol. 10, pp. 28572–28581, 2018.

[18] J. K. Nørskov, J. Rossmeisl, A. Logadottir, L. Lindqvist, D.- Lyngby, and H. Jo, “Origin of the Overpotential for Oxygen Reduction at a Fuel-Cell Cathode,” pp. 17886–17892, 2004.

[19] A. A. Peterson, F. Abild-pedersen, F. Studt, J. Rossmeisl, and J. K. Nørskov, “How copper catalyzes the electroreduction of carbon dioxide into hydrocarbon fuels †,” pp. 1311–1315, 2010.

[20] W. Meteorological and O. Wmo, “The Global Climate in 2015 – 2019,” 2019.

[21] E. I. Pathways, “World Energy Scenarios 2019,” 2019.

[22] MoARD, “Performance of Ethiopian Agriculture Sector.” 2010.

[23] D. P. Series, “Environment for Development The Impact of CO_2 Emissions on Agricultural Productivity and Household Welfare in Ethiopia.”

[24] H. Zhou *et al.*, “Journal of Colloid and Interface Science Recent advances in different-dimension electrocatalysts for carbon dioxide reduction,” *J. Colloid Interface Sci.*, vol. 550, no. May 2018, pp. 17–47, 2019.

[25] “Mechanistic Pathway in the E lectrochemical R eduction of CO_2 on RuO_2,” 2015.

[26] Xuping Sun, “Highly Selective Electrochemical Reduction of CO_2 to Alcohols on FeP Nanoarray,” 2019.

[27] J. Kehlet, “Trends in the exchange current for hydrogen evolution,” 2005.

[28] J. W. Evans, “Introduction and the Signi fi cance of Electrometallurgy,” vol. 2014, no. April 2015, pp. 1–13, 2016.

[29] C. Cui, H. Wang, X. Zhu, J. Han, and Q. Ge, “A DFT study of CO_2 electrochemical reduction on Pb (211) and Sn (112),” 2015.

[30] J. Wu, Y. Huang, W. Ye, and Y. Li, “CO_2 Reduction : From the Electrochemical to Photochemical Approach,” vol. 1700194, pp. 1–29, 2017.

[31] Z. Yin, G. T. R. Palmore, and S. Sun, “Electrochemical Reduction of CO_2 Catalyzed by Metal Nanocatalysts,” *Trends Chem.*, vol. 1, no. 8, pp. 739–750, 2019.

[32] R. Jern *et al.*, “A review on the electrochemical reduction of CO_2 in fuel cells , metal electrodes and molecular catalysts,” *Catal. Today*, vol. 233, pp. 169–180, 2014.

[33] P. Shao, S. Ci, L. Yi, P. Cai, P. Huang, and C. Cao, “Hollow CuS Microcubes Electrocatalysts for CO 2 Reduction Reaction.”

[34] B. M. Abraham and G. Vaitheeswaran, “DFT study of the formate formation on Ni (111) surface doped by transition metals [Ni (111) -M ; M = Cu , Pd , Pt , Rh],” no. 111, 2016.

[35] Z. Jiang, T. Xiao, V. L. Kuznetsov, and P. P. Edwards, “Turning carbon dioxide into fuel,” no. June, 2010.

[36] J. S. Yoo, R. Christensen, T. Vegge, K. N, and F. Studt, “Theoretical Insight into the Trends that Guide the Electrochemical Reduction of Carbon Dioxide to Formic Acid,” pp. 358–363, 2016.

[37] Y. Takeuchi, “A refinement of the crystal structure of covellite , CuS,” vol. 8, no. 6, 1977.

[38] A. Soares and A. Morales-garcia, “The Stability and Structural , Electronic and Topological Properties of Covellite (001) Surfaces .,” no. July, 2016.

[39] A. L. S. Jr, E. C. Dos Santos, T. Heine, and H. A. De Abreu, “Two-dimensional crystal CuS—electronic and structural properties,” *2D Mater.*, vol. 4, no. 1, pp. 1–7.

[40] R. Gaspari, L. Manna, A. Cavalli, R. Gaspari, L. Manna, and A. Cavalli, “A theoretical investigation of the (0001) covellite surfaces,” vol. 044702, no. 0001, 2014.

[41] B. R. Tagirov, A. L. Trigub, and K. O. Kvashnina, “ScienceDirect Covellite CuS as a matrix for ‘‘ invisible ’’ gold : X-ray spectroscopic study of the chemical state of Cu and Au in synthetic minerals,” *Geochim. Cosmochim. Acta*, vol. 191, no. August, pp. 58–69, 2016.

[42] A. L. S. Jr, E. C. Dos Santos, T. Heine, and H. A. De Abreu, “Two-dimensional crystal CuS—electronic and structural properties,” vol. 015041.

[43] C. Cus, A. Morales-garc, A. L. Soares, E. C. Dos Santos, and H. A. De Abreu, “First-Principles Calculations and Electron Density Topological Analysis of Covellite (CuS),” no. November 2017, 2014.

[44] A. Morales-garc, A. L. Soares, E. C. Dos Santos, H. A. De Abreu, and A. Duarte, “First-Principles Calculations and Electron Density Topological Analysis of Covellite (CuS),” 2014.

[45] C. Dong, M. Ji, X. Yang, J. Yao, and H. Chen, “Formaldehyde Catalyzed by Hourglass Ru ,” vol. 2.

[46] Y. S.-H. Katherine Reece Phillips, Yu Katayama, Jonathan Hwang, “Sulfide-derived Copper for Electrochemical Conversion of CO 2 to Formic Acid,” 2018.

[47] N. Q. Su and X. Xu, “Development of New Density Functional Approximations,” 2017.

[48] J. A. S. DAVID S. SHOLL, *Density Functional Theory*. WILEY, 2009.

[49] V. Sahni, “Hohenberg and Kohn-Sham Density Functional Theory,” pp. 11–12, 2004.

[50] J. P. Perdew, K. Burke, and M. Ernzerhof, “Generalized Gradient Approximation Made Simple,” no. 3, pp. 3865–3868, 1996.

[51] G. Kresse and D. Joubert, “From ultrasoft pseudopotentials to the projector augmented-wave method,” vol. 59, no. 3, pp. 11–19, 1999.

[52] P. Schwerdtfeger, “The Pseudopotential Approximation in Electronic Structure Theory,” pp. 3143–3155, 2011.

[53] Wikipedia, “Pseudopotential.” https://en.wikipedia.org/wiki/Pseudopotential.

[54] G. R. Schleder, A. C. M. Padilha, C. M. Acosta, and M. Costa, “From DFT to machine learning : recent approaches to materials science – a review,” *J. Phys. Mater.*, vol. 2, no. 3, p. 32001, 2019.

[55] P. Giannozzi *et al.*, "Q UANTUM ESPRESSO : a modular and open-source software project for quantum simulations of materials," vol. 395502, 2009.

[56] Q.- Espresso, C. M. Dynamics, and F. M. Dynamics, "Lab 2 : Handout Quantum-Espresso : a first-principles code," pp. 1–20, 2005.

[57] G. Kresse and M. Marsman, "Vienna ABinitio Package Simulation VASP," 2018.

[58] "VESTA : A Three-Dimensional Visualization System for Electronic and structural analysis," no. June 2008, 2014.

[59] M. Meunier, "Introduction to Materials Studio," no. June 2012, 2016.

[60] C. J. Cramer, *Essentials of Computational Chemistry:2009* .

[61] M. J. S. Spencer, "DFT modelling of hydrogen on CU (110) - and (111)," no. August 2002, 2014.

[62] Smooth and T. Ha. E. Step, "High-precision sampling for Brillouin-zone integration in metals M.," vol. 40, no. 6, pp. 3616–3621, 1989.

[63] H. J. Monkhorst and J. D. Pack, "Special points for Brillonin-zone integrations* Hendrik," vol. 13, no. 12, pp. 5188–5192, 1976.

[64] Á. Morales-garcía and J. He, "Surfaces and morphologies of covellite (CuS) nanoparticles by means of ab initio atomistic thermodynamics," *CrystEngComm*, no. 001, 2017.

[65] Y. Takéuchi, Y. Kudoh, and G. Sato, "The crystal structure of covellite CuS under high pressure Up to 33 kbar," vol. 1985, pp. 119–128, 1985.

[66] J. G. C. & F. J. Qi Lu1,*, Jonathan Rosen1,*, Yang Zhou2, Gregory S. Hutchings1, Yannick C. Kimmel1, "A selective and efficient electrocatalyst for carbon dioxide reduction," pp. 1–6, 2014.

[67] I. S. Kwon, T. Debela, H. Kwak, W. Seo, and K. Park, "Selective Electrochemical Reduction of Carbon dioxide to Formic Acid Using Indium-Zinc Bimetallic Nanocrystals," pp. 1–30, 2019.

[68] M. Ghoussoub, "First Principles Investigation of Heterogeneous Catalysis," 2016.

[69] Y. Deng *et al.*, "On the Role of Sulfur for the Selective Electrochemical Reduction of CO_2 to Formate on CuS x Catalysts," 2018.